University of Alberta

Damage Study of a Rubber-Toughened Polymer under Biaxial Fatigue Loading

by

Hyock-Ju Kwon

A thesis submitted to the Faculty of Graduate Studies and Research in partial fulfillment of the requirements for the degree of *Master of Science*

Department of Mechanical Engineering

Edmonton, Alberta

Fall, 2003

National Library of Canada
Acquisitions and Bibliographic Services
395 Wellington Street
Ottawa ON K1A 0N4
Canada

Bibliothèque nationale du Canada
Acquisisitons et services bibliographiques
395, rue Wellington
Ottawa ON K1A 0N4
Canada

Your file Votre référence
ISBN: 0-612-87806-6
Our file Notre référence
ISBN: 0-612-87806-6

The author has granted a non-exclusive licence allowing the National Library of Canada to reproduce, loan, distribute or sell copies of this thesis in microform, paper or electronic formats.

The author retains ownership of the copyright in this thesis. Neither the thesis nor substantial extracts from it may be printed or otherwise reproduced without the author's permission.

L'auteur a accordé une licence non exclusive permettant à la Bibliothèque nationale du Canada de reproduire, prêter, distribuer ou vendre des copies de cette thèse sous la forme de microfiche/film, de reproduction sur papier ou sur format électronique.

L'auteur conserve la propriété du droit d'auteur qui protège cette thèse. Ni la thèse ni des extraits substantiels de celle-ci ne doivent être imprimés ou aturement reproduits sans son autorisation.

Canada

University of Alberta

Library release form

Name of Author: *Hyock-Ju Kwon*

Title of Thesis: *Damage Study of a Rubber-Toughened Polymer under Biaxial Fatigue Loading*

Degree: *Master of Science*

Year this Degree Granted: *2003*

Permission is hereby granted to the University of Alberta Library to reproduce single copies of this thesis and lend or sell such copies for private, scholarly, or scientific research purposes only.

The author reserves all other publication and other rights in association with the copyright in the thesis, and except as hereinbefore provided, neither the thesis nor any substantial portion thereof may be printed or otherwise reproduced in any material form whatever without the author's prior written permission.

August 8, 2003

University of Alberta

Faculty of Graduate Studies and Research

The undersigned certify that they have read, and recommended to the Faculty of Graduate Studies and Research for acceptance, a thesis entitled *Damage Study of Polymer under Biaxial Fatigue Loading* submitted by *Hyock-Ju* Kwon in partial fulfillment of the requirements for the degree *of Master of Science.*

Dr. U. Sundararaj

Dr. T. W. Forest

Dr. Z. Xia

Aug. 8/2003

Dr. P.-Y. B. Jar

Abstract

Toughness variation of non-notched poly(acrylonitrile-butadiene-styrene) (ABS) subjected to uniaxial and biaxial fatigue loading was investigated. Fatigue loading was introduced to strip and cruciform specimens for uniaxial and biaxial loadings, respectively. Toughness of the specimens were then evaluated using tensile test from which the fracture strain, named cracking strain here, was used to monitor the toughness change.

The mechanical test results showed that the toughness drop occurred in ABS under fatigue loading, even before any visible crack was developed. However, the uniaxial stress had more significant effect than the biaxial stress on the toughness drop.

Damage development and fracture behavior were analyzed using scanning electron microscopy. The analysis revealed that damage zones initiated during the fatigue loading were the main cause of the toughness drop. The damage zones consisted of crazes and bridging large rubber particles, which were yet to develop to a crack.

The study concludes that the addition of the transverse stress to ABS, i.e. biaxial loading, increases its toughness for the fatigue resistance.

Acknowledgements

I am particularly indebted to my supervisors, Dr. P.-Y. Ben Jar and Dr. Zihui Xia for their guidance and financial support throughout this study. I am also grateful to them for their invaluable advice and discussions for this thesis.

I also wish to thank Mr. Bernie Faulkner, Mr. Dave Pape, and Mr. Albert Yuen who offered me the excellent technical help and valuable discussions.

Appreciation is also extended to Dr. Don Raboud for early development of the bi-axial testing rig. In addition, I would like to thank the members of the Durable Materials Research Lab: Dr. Takashi Kuboki, Mr. Emran Rashed and Mr. Yemi Setiadi for their friendship and provision of a pleasant environment.

Special thanks go out to NSERC for the financial support throughout the study.

Finally, my gratitude must be given to my wife, H. E. Chun, for her supporting me and believing in me throughout the study, as well as my life.

CONTENTS

1. Introduction **1**

1.1 Toughness 4

1.1.1 Energy release rate 6
1.1.2 Stress intensity factor 8
1.1.3 Crack tip opening displacement (CTOD) 11
1.1.4 J-Integral 12
1.1.5 Essential work 14

1.2 Rubber-toughened polymers 15

1.3 ABS 17

1.4 Deformation and fracture of polymers 19

1.5 Biaxial tests 21

2. Test Methodology **28**

2.1 Uniaxial fatigue test 29

2.1.1 Test specimens 29
2.1.2 Procedure for the specimen preparation 30
2.1.3 Fatigue tests 30

2.2 Biaxial fatigue test 32

2.2.1 Test rig 32
2.2.2 Design of test specimens 34
2.2.3 Procedure for the specimen preparation 35
2.2.4 Load cell calibration 35
2.2.5 Fatigue test 37

2.3 Tensile test 37

2.3.1 Test specimens 37
2.3.2 Specimen preparation 38
2.3.3 Tensile test 39

3. FEM Modeling **40**

3.1 FEM model 40

3.2 Stress analysis with original thickness 41

3.3 Stress analysis with reduced thickness 43

4. Effect of Fatigue Loading on Mechanical Properties 46

4.1 Introduction 46

4.2 Cracking strain 46

4.3 Mechanical test results 48

4.4 Micro-structural analysis 53

4.4.1 Fracture deformation 53
4.4.2 Shear yielding and crazing 54
4.4.3 Damage zone 61
4.4.4 Toughness variation by fatigue loading 65
4.4.5 Summary 68

5. Conclusions 70

6. Recommendations for the future studies 72

7. Bibliography 73

List of Figures

Fig. 1.1 A through thickness crack in an infinitely wide plate subjected to a remote tensile stress. 7

Fig. 1.2 Definition of the coordinate axes ahead of a crack tip (Anderson) 9

Fig. 1.3 The three loading modes that can be applied to a crack (Anderson) 10

Fig. 1.4 Estimation of CTOD from the displacement of an effective crack (Anderson). 12

Fig. 1.5 Arbitrary contour around the tip of a crack (Anderson) 13

Fig. 1.6 The deep edge notched specimen 15

Fig. 1.7 Stress-strain curves for rubber-toughened polymers (Young and Lovell). 17

Fig. 1.8 A graphical representation of the basic structure of ABS (Lee) 18

Fig. 1.9 A typical stress-strain curve for ABS 18

Fig. 1.10 (a) Shear yielding under tension (Bucknall), and (b) Sample of polycarbonate containing several crazes (Young and Lovell) 20

Fig. 1.11 (a) Specimen and (b) its fringe pattern under uniaxial force (Mönch and Galster). 21

Fig. 1.12 (a) Specimen, and (b) test equipment used (Kelly). 24

Fig. 1.13 Cruciform specimen (Leevers et al). 26

Fig. 1.14 (a) Specimen, and (b) test equipment (Atkins et al). 27

Fig. 2.1 Procedure for toughness evaluation under uniaxial and biaxial fatigue loadings. 29

Fig. 2.2 10,000 lbf MTS machine, series 812 31

Fig. 2.3 4-axis biaxial test rig 33

Fig. 2.4 Front view of the design drawing of the biaxial test rig 33

Fig. 2.5 Cruciform specimen: (a) the dimension, including thickness reduction in the centre, and (b) a photograph of a machined specimen 34

Fig. 2.6 (a) Drilling jig, and (b) milling jig for cruciform specimen. 35

Fig. 2.7 Dog-bone calibrator 36

Fig. 2.8 Dog-bone type tensile test specimen 38

Fig. 2.9 Cutting plan of (a) cruciform specimen, and (b) strip specimen. 39

Fig. 2.10 (a) Milling jig with specimen, and (b) Polishing jig for width reduction in the gauge section. 39

Fig. 3.1 FEM model of a quarter of specimen 41

Fig. 3.2 FEM contour plot showing the distribution of the 1st principal stress in the cruciform specimen under equi-biaxial loading 42

Fig. 3.3 Stress variation along the stress path given in Fig. 3.2..... 43

Fig. 3.4 Plan for thickness reduction in cruciform specimen (unit: mm) 44

Fig. 3.5 FEM results showing the 1st and 2nd principal stresses along the path given in Fig. 3.4. 44

Fig. 3.6 Cross-sectional view of reduced thickness (unit: mm)..... 45

Fig. 3.7 Cutting plan of the cruciform specimen with reduced thickness..... 45

Fig. 4.1 Tensile stress-strain behaviors of non-fatigued and fatigued ABS. 47

Fig. 4.2 Variation of cracking strain with uniaxial fatigue loading. 49

Fig. 4.3 Variation of cracking strain with uniaxial and biaxial fatigue loading. 51

Fig. 4.4 Four phases of fracture development under fatigue loading 54

Fig. 4.5 SEM micrograph of tensile fractured surface, after 500 cycles of uniaxial fatigue loading at 25MPa (From specimen F-1) 55

Fig. 4.6 SEM micrographs of fractured surface of an ABS specimen, from region A in Fig. 4.5. 55

Fig. 4.7 Deformation sequence in front of the crack tip in rubber toughened polymers. 56

Fig. 4.8 SEM micrographs of the shear yielding dominated region of an ABS specimen fractured under pure tension 57

Fig. 4.9 SEM micrograph of a shear yielding dominated region of an ABS specimen fractured under pure tension. 58

Fig. 4.10 SEM micrographs of fractured surface of an ABS specimen, from region B in Fig. 4.5..... 58

Fig. 4.11 Failure envelopes for PMMA under biaxial stress showing crazing and shear yielding (Raghava et al.) 60

Fig. 4.12 SEM micrograph of fractured surface of an ABS specimen, from region C in Fig 3.5..... 62

Fig. 4.13 Deformation model of a damage zone during the fatigue loading..... 63

Fig. 4.14 Craze formation in glassy polymers. (Anderson)..... 63

Fig. 4.15 SEM micrograph of a fractured surface from a purely tensile fractured ABS specimen (F-2) after 500 cycles of uniaxial fatigue loading at 25MPa..... 66

Fig. 4.16 Stress distribution, σ_r and σ_θ, around the circular hole under the uniaxial loading..... 67

Fig. 4.17 Distribution of σ_θ along the edge of the hole under uniaxial loading (——) and biaxial loading (-------). 68

1. Introduction

The discipline of fracture mechanics has increasingly influenced design and experimental work involving the fatigue life prediction of flawed structural components. The mathematical and physical models used to rationalize material toughness data, however, generally concentrate on uniaxial stress environment, in which the transverse stress is assumed to be secondary and, in some cases, irrelevant.

On the other hand, it is recognized in most working structures that the stress state is not simple uniaxial. Biaxial and triaxial stress states often exist. Thus it is necessary to know how the toughness changes under complex stress states. The question often starts with whether a bi-axial stress state will change the toughness or the crack initiation and growth processes. In the case of buckling, it was mathematically proven by Timosenko [1] that the addition of tensile transverse loading increases and the compressive loading decreases the critical buckling load. But the buckling model cannot be applied to tensile fracture and very few mathematical models were proposed to predict the effect of the transverse loading on the tensile fracture.

While the effects of biaxial stress state have been studied experimentally for many metals [2], very little information is available for polymers, especially under low and high cyclic fatigue. Standard tests on polymers [3,4] have essentially no information of this kind. Moreover, linear elastic fracture mechanics theory states that, in a biaxial stress

field, the stress parallel to the crack direction does not contribute to the crack growth [5]. Among the small number of researchers who studied the effect of a biaxial stress state, Leevers and his co-workers [6,7] looked at crack growth behavior of poly-methyl methacrylate (PMMA) and polyvinylchloride (PVC) under high frequency fatigue loading, where da/dN (crack propagation rate) for PMMA reduced somewhat under tensile biaxialities while the effects of biaxiality were almost absent for PVC. Takemori [8] investigated biaxial fatigue of polycarbonate discs impacted by a plunger, data from which were analyzed in traditional terms of fatigue stress versus number of cycles. Atkins and co-workers [9] used ABS (poly(acrylonitride butadiene styrene)) and PVC sheets to investigate the effect of biaxiality on the toughness and the crack propagation rate. They concluded that toughness in the direction perpendicular to the crack is least under equi-biaxial tension while it is greatest under uni-axial tension.

Apart from the above limited studies, there are virtually no studies devoted to the biaxial fracture of polymers. This lack of data is rather surprising given the known effects of biaxiality on fracture and fatigue of metals [10,11,12,13]. The lack of information makes one wonder whether proper criteria have been used in the design of polymer products such as pipelines, shell structures, pressure vessels, container storage vessels which operate under biaxial loading. It is often assumed that the transverse stress has no effect on fracture and fatigue, yet the presence of an applied transverse stress can remarkably change the shape of the in-plane shear stress contours in the vicinity of the crack tip [14]. This change of the stress state affects molecular orientation patterns at crack tips and thus crack initiation and propagation.

As discussed above, the paucity of the data under biaxial stresses can hardly be a

result of disinterest. Rather it is partly due to the practical difficulties in testing. The problem is further aggravated by the lack of standards for the biaxial testing. This study, even more than 20 years after the first biaxial test on polymers was reported, is one of a handful of studies that intend to elucidate the toughness change under biaxial fatigue loading.

Most of the studies of the fatigue behavior use the resistance to crack propagation for the toughness measurement, for which the pre-cracked specimens are used. Crack development in a fatigue loading process can be split into four stages[15]: (i) crack initiation, (ii) crack growth in the direction of maximum shear stress (stage I fracture), (iii) crack growth in the direction of maximum tensile stresses (stage II fracture) and (iv) final fracture or rupture. To study the fatigue-crack behavior, two kinds of specimen geometries are used under the uniaxial fatigue loading: plain smooth specimens of hour-glass shape (non-notched specimen) subjected to push-pull cyclic loading, and flat-plate notched specimens subjected to cyclic stress with a tensile mean stress. The former leads to understanding of crack initiation and early growth. The latter allows quantitative assessment of crack growth up to the final failure. Most of the previous studies have focused on stage I fracture (crack growth) and used the notched specimens for testing. These studies assume that no property change occurs before crack initiation even under a prolonged fatigue loading; however, this assumption has never been verified. In this study, fatigue load was firstly introduced to the non-notched plain smooth specimens, but without generating any crack or visible damage. Then, pure tensile test was carried out on the fatigued specimens to evaluate the change in toughness for crack initiation under fatigue loading. By doing so, we examine the assumption of the previous studies

mentioned above for rubber toughened polymer, and this is one of the other purposes of this study.

The objectives of the current study can be summarized as follows:

(a) to evaluate the toughness changes under fatigue loading before any crack or visible damages is initiated, and

(b) to compare the toughness changes under uniaxial and biaxial fatigue loadings.

The toughness evaluation was based on specimens of dog-bone shape (non-notched specimens). Special attention was paid to make sure that no crack or visible whitening occurred in the specimens by the fatigue loading.

The remainder of Chapter 1 introduces basic theories of toughness, background of rubber- toughened polymers and conventional bi-axial tests. Chapter 2 describes the testing procedure and methodology used in this study. Chapter 3 discusses the effect of uniaxial and biaxial fatigue loadings on the toughness and the microstructure of the material. Chapter 4 is devoted to the conclusions drawn from this work and indicates how this study is related to engineering design and analysis. The final chapter recommends work for the future studies.

1.1 Toughness

Toughness is a measure of material's resistance to failure. Used with the prefix "fracture", it refers to the energy per unit area needed to generate a new crack surface. The concept of linear elastic fracture mechanics (LEFM) that was derived prior to 1960 is applicable only to materials that obey Hooke's Law. Although modifications were later made to accommodate small-scale plasticity, these analyses are still restricted to

structures whose global behavior is linear elastic. For example, energy release rate and stress intensity factor are two measures of the fracture toughness in the global deformation behavior that can be well described using LEFM.

Since LEFM is valid only if nonlinear material deformation is confined to a small region surrounding the crack tip, fracture behaviors of many materials are virtually impossible to characterize using LEFM due to their elastic-plastic deformation, and nonlinearity between stress and strain, sometimes even in the global elastic range. For these types of materials, crack tip opening displacement (CTOD) and J-integral are used to characterize the crack growth resistance, each of which can be used as a fracture criterion.

For ductile materials, the total work to fracture is not a material property [16]. Only the work performed in the end region of a crack tip, where the fracture process takes place, is constant for a given thickness, and is known as the essential work of fracture.

All the above-mentioned toughness measures are estimated using specimens with a pre-existing crack, results from which provide the fracture criteria for the crack growth. In contrast, experimental study conducted in this work used specimens without any visual crack. Therefore, the current study is focused on the change of the toughness for crack initiation.

As to be shown later in Section 3, the total strain to fracture can be used as a measure of toughness for un-notched dog-bone specimens. The fracture strain is named "cracking strain" here, and is used to characterize the toughness change of the rubber-toughened polymer due to the cyclic loading.

1.1.1 Energy release rate

In 1920, Griffith [17] proposed that a crack can form (or an existing crack can grow) only if such a process does not cause the increase of the total energy. Thus the critical condition for fracture can be defined as the point where crack growth occurs under equilibrium conditions, with no net change in total energy.

Consider a plate that contains a crack of 2a in length and is subjected to a constant stress, σ, that is perpendicular to the crack length direction (Fig. 1.1), in which the plate width is much larger than $2a$ and plane stress conditions prevail. In order for this crack to increase in size, sufficient potential energy must be available to overcome the required surface energy for crack growth in the material. The Griffith energy criterion for an incremental increase in the crack area, dA, under equilibrium conditions can be expressed in the following way:

$$\frac{dW}{dA} = \frac{d\Pi}{dA} + \frac{dS}{dA} = 0 \qquad (1.1)$$

where W is the total energy, Π is the potential energy supplied by the internal strain energy and external forces, and S is the work required to create new surfaces. For the cracked plate illustrated in Fig. 1.1, Griffith used the stress analysis of Inglis [18] to show that

$$\Pi = \Pi_0 - \frac{\pi\sigma^2 a^2 B}{E} \qquad (1.2)$$

where Π_0 is the potential energy of an un-cracked plate, E is Young's modulus, and B is the plate thickness. Since the formation of a crack requires the creation of two surfaces, S is given by

$$S = 4aB\gamma_s \tag{1.3}$$

where γ_s is the surface energy per unit area of the material.

Since $dA = 2Bda$,

$$-\frac{d\Pi}{dA} = \frac{\pi\sigma^2 a}{E} \tag{1.4}$$

and

$$\frac{dS}{dA} = 2\gamma_s \tag{1.5}$$

Equating (1.4) and (1.5) and solving for fracture stress gives

$$\sigma_f = \left(\frac{2E\gamma_s}{\pi a}\right)^{1/2} \tag{1.6}$$

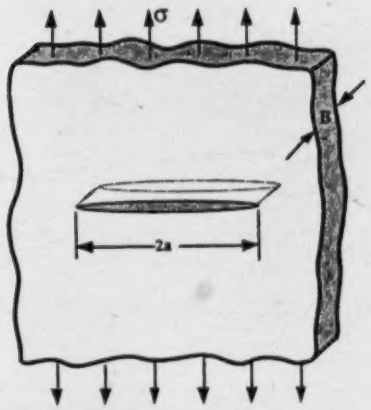

Fig. 1.1 A through thickness crack in an infinitely wide plate subjected to a remote tensile stress. (Anderson [19])

Similarly in 1956, Irwin [20] proposed an energy approach for fracture, and defined an *energy release rate*, G, which is a measure of the minimum energy required for an increment of crack area:

$$G = -\frac{d\Pi}{dA} \tag{1.7}$$

The term *rate* used in this context does not refer to a derivative with respect to time; and G is the rate of change in potential energy with crack area. Since G is obtained from the derivative of a potential energy with respect to the crack area, it is also called the *crack extension force* or the *crack driving force*. According to (1.4), the energy release rate for a wide plate in plane stress with a crack of length $2a$ (Fig. 1.1) is given by

$$G = \frac{\pi\sigma^2 a}{E} \tag{1.8}$$

Crack extension occurs when G reaches a critical value,

$$G_c = \frac{dS}{dA} = 2(\gamma_s + \gamma_p) \tag{1.9}$$

where G_c is a measure of the fracture toughness of the material, γ_p is the plastic work per unit area of surface created, and is typically much larger than γ_s. The generalized fracture stress from Eq. (1.8) and Eq. (1.9) is

$$\sigma_f = \left(\frac{2Ew_f}{\pi a}\right)^{1/2} \tag{1.10}$$

where w_f is the fracture energy which could include plastic, visco-elastic, or visco-plastic effects depending on the material. For the ideally brittle material, $w_f = \gamma_s$.

1.1.2 Stress intensity factor

For certain cracked configurations subjected to external forces, it is possible to derive closed-form expressions for stresses in the body, assuming isotropic linear elastic

material behavior, as reported by Westergaard [21] and Williams [22]. Using polar coordinates with the origin at the crack tip (Fig. 1.2), it can be shown that the stress field ahead of a crack in an elastic body is given by

$$\sigma_{ij} = \left(\frac{k}{\sqrt{r}}\right) f_{ij}(\theta) + \sum_{m=0}^{\infty} A_m r^{\frac{m}{2}} g_{ij}^{(m)}(\theta) \qquad (1.11)$$

where σ_{ij} is the stress tensor, k is a constant, and f_{ij} is a dimensionless function of θ. As $r \to 0$, the leading term approaches infinity, but the other terms remain finite or approach zero. Thus stress near the crack tip varies with $1/\sqrt{r}$, regardless of the configuration of the cracked body. It can also be shown that displacement near the crack tip varies with $\sqrt{r}$[9].

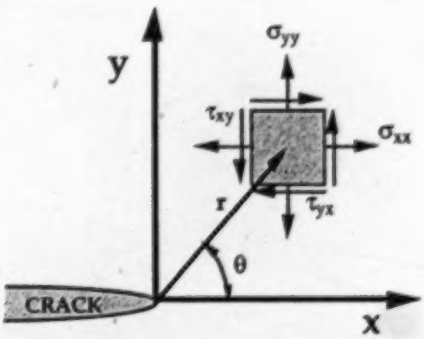

Fig. 1.2 Definition of the coordinate axes ahead of a crack tip (Anderson [19])

There are three loading modes that a crack can experience, as Fig. 1.3 illustrates. Each loading mode produces the $1/\sqrt{r}$ singularity at the crack tip, but the proportionality constant k and f_{ij} depend on loading mode. k can be replaced by the stress intensity factor, K, where $K = k\sqrt{2\pi a}$. The stress intensity factor is usually given a subscript to

denote the mode of loading, i.e. K_I, K_{II}, and K_{III}. Thus the stress fields ahead of a crack tip in an isotropic linear elastic material can be written as

$$\lim_{r\to 0}\sigma_{ij}^{(I)} = \frac{K_I}{\sqrt{2\pi r}} f_{ij}^{(I)}(\theta) \qquad (1.12)$$

$$\lim_{r\to 0}\sigma_{ij}^{(II)} = \frac{K_{II}}{\sqrt{2\pi r}} f_{ij}^{(II)}(\theta) \qquad (1.13)$$

$$\lim_{r\to 0}\sigma_{ij}^{(III)} = \frac{K_{III}}{\sqrt{2\pi r}} f_{ij}^{(III)}(\theta) \qquad (1.14)$$

for Modes I, II, and III, respectively. In a mixed mode of loading, the individual contributions to a given stress component are additive:

$$\sigma_{ij}^{(total)} = \sigma_{ij}^{(I)} + \sigma_{ij}^{(II)} + \sigma_{ij}^{(III)} \qquad (1.15)$$

Detailed expressions for the singular stress fields can be found in many references (e.g. [23]) in the field of fracture mechanics.

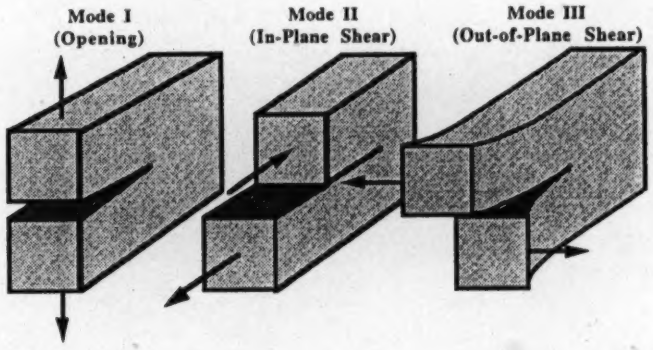

Fig. 1.3 The three loading modes that can be applied to a crack (Anderson [19])

The stress intensity defines the amplitude of the crack tip singularity, as stresses near the crack tip are proportional to K. Moreover, the stress intensity factor completely defines the crack tip condition; if K is known, it is possible to solve for all components of stresses and displacements as functions of r and θ (e.g. [24]).

1.1.3 Crack tip opening displacement (CTOD)

Both energy release rate and stress intensity factor are based on LEFM which is valid only if nonlinear material deformation is confined to a small region surrounding the crack tip. For many materials, it is virtually impossible to characterize the fracture behavior using the concept of LEFM, thus an alternative fracture mechanics model is required. Elastic-plastic fracture mechanics can be applied to materials that exhibit time-independent, non-linear behavior (i.e., plastic deformation [25]). Two elastic-plastic parameters are discussed here: the crack tip opening displacement (CTOD) and the J-contour integral [26]. Both parameters describe crack tip conditions in elastic-plastic materials, and each can be used as a fracture toughness criterion.

The CTOD concept was first proposed by Wells [27] who noticed that the crack faces had moved apart prior to fracture while examining test specimens; plastic deformation blunted an initially sharp crack. The degree of crack blunting is proportional to the toughness of the material, thus can be used as a toughness measure.

In a small scale yielding, it can be shown that CTOD (δ) in Fig 1.4 is related to energy release rate (G) and stress intensity factor (K_I) as

$$\delta = 2u_y = \frac{4}{\pi}\frac{K_I^2}{\sigma_{YS}E} = \frac{4}{\pi}\frac{G}{\sigma_{YS}} \qquad (1.16)$$

where σ_{YS} is yield strength, and E is Young's modulus. Wells postulated that CTOD is an appropriate crack tip characterizing parameter when LEFM is no longer valid and this assumption was shown to be correct later.

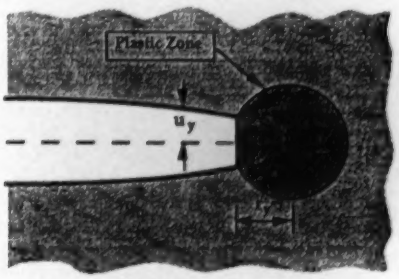

Fig. 1.4 Estimation of CTOD from the displacement of an effective crack (Anderson [19])

1.1.4 J-Integral

As presented by Rice [28], J-integral is a contour integral for analysis of energy required for crack growth. Rice showed that the value of this integral, which he called J, is equal to the energy release rate in a nonlinear elastic body that contains a crack. Considering an arbitrary counter-clockwise path (Γ) around the tip of a crack, as illustrated in Fig. 1.5, the J-integral is given by:

$$J = \int_{\Gamma} (w dy - T_i \frac{\partial u_i}{\partial x} ds) \qquad (1.17)$$

where w is the strain energy density, T_i components of the traction vector, u_i the displacement vector components, and ds a length increment along the contour Γ. The strain energy density w is defined as

$$w = \int_0^{\varepsilon_{ij}} \sigma_{ij} d\varepsilon_{ij} \qquad (1.18)$$

where σ_{ij} and ε_{ij} are the stress and strain tensors, respectively. The traction vector (T_i) is a stress vector normal to the contour and is given by

$$T_i = \sigma_{ij} n_j \qquad (1.19)$$

where n_j are the components of the unit vector normal to Γ. Rice showed that the value of the J-integral is independent of the path of integration around the crack. Thus J is also called a *path-independent* integral.

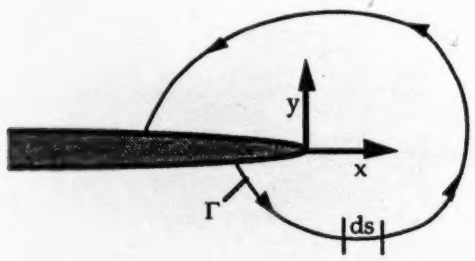

Fig. 1.5 Arbitrary contour around the tip of a crack (Anderson [19])

Rice also showed that J-integral is equivalent to the energy release rate in a nonlinear elastic body that contains a crack. That is

$$J = -\frac{d\Pi}{dA} \qquad (1.20)$$

where Π is the potential energy and A the crack area. The potential energy is the difference between the strain energy and the work done by external forces. Mathematically, it is expressed as

$$\Pi = U - F \qquad (1.21)$$

Thus, Eq. (1.20) is the same as the definition for the energy release rate, (1.7), except that G is replaced by J.

In summary, J-integral is a measure of fracture toughness [29,30] for nonlinear elastic plastic materials, as energy release rate G does for linear elastic material.

1.1.5 Essential work

Borberg [31,32,33] has suggested a different approach to characterize toughness at the crack tip, which is to divide the crack into an end region where the fracture process takes place, and an outer region where screening plastic deformation is necessary to accommodate the large strains in the end region. For brittle materials, the plastic deformation in the screening region is small and the Griffith-Orowan theory [34] is sufficient to describe the mechanics of the fracture process. However, in more ductile materials, the region of screening plastic deformation is large, compared with that in the end region. In the case of ductile fracture in thin sheets, the end region can be identified with the necking behavior. It is only the work performed in this end region that is essential for the crack growth. Thus this part of energy is called essential work of fracture, and is shown to be a material constant [35]. On the other hand, the plastic deformation in the outer region depends on the particular geometry of the specimen, and the associated plastic work is not an autonomous material constant.

If a deep edge-notched sheet specimen (Fig. 1.6) yields completely before fracture, the plastic region around the crack tip is almost circular with the ligament (length l) as diameter. Thus although there is general yielding, the plastic region is confined. The work preformed to fracture such a specimen can be separated into two components:

(i) The essential work performed in the end region.

(ii) The non-essential work performed in the screening plastic region.

The essential work is proportional to the ligament length l, if it is assumed that the specific essential work remains constant. The non-essential work in the rest of the plastic region is proportional to l^2. If w_p represents the specific non essential work, defined as

the plastic work in a specimen with unit thickness and ligament length l, then the total work of fracture can be written as

$$W_f = ltw_e + l^2 tw_p \qquad (1.22)$$

where w_e is the essential work, and t the sheet thickness. Thus, if the specific work of fracture $w_f = W_f / lt$ is plotted against the ligament length l, there should be a straight line with a positive intercept that is the specific essential work w_e. Eq. (1.22) is valid only if complete yielding of the ligament section occurs before crack growth is initiated, and if the ligament is in a plane stress state.

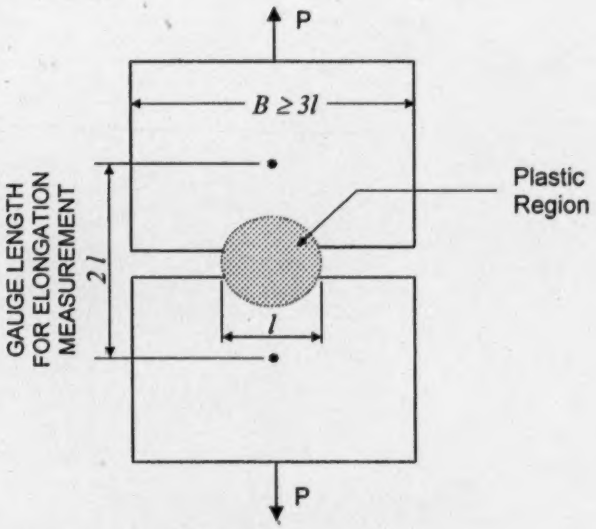

Fig. 1.6 The deep edge notched specimen

1.2 Rubber-toughened polymers

Poly(acrylonitrile-butadiene-styrene) (ABS) is a rubber-toughened glassy polymer. Glassy polymers, in general, have strength that is adequate for many applications but they

are prone to fracture in a brittle manner, particularly when notched or subjected to impact loading. Because of such problems, rubber-toughened polymers have been developed to reduce the notch sensitivity and to increase the toughness. In rubber-toughened polymers, rubber particles form a second phase surrounded by a continuous phase of glassy polymer matrix. The inclusion of rubber particles can lead to significant improvements of the ductility and toughness.

The profound effect of incorporating rubber particles into a brittle polymer upon the mechanical properties is demonstrated in Fig. 1.7. The stress-strain curve for polystyrene (PS), Fig. 1.7(a), shows brittle behavior, whereas the inclusion of the rubbery phase, high impact polystyrene (HIPS) also in Fig. 1.7(a), allows the material to undergo yielding and deform plastically to 40% of strain before fracture occurs. The plastic deformation is often accompanied by 'stress-whitening' which becomes more intense as the test proceeds. This is due to the formation of a large number of crazes in the matrix around the rubber particles [36]. It should be noted that there was no sign of necking in HIPS.

In addition to HIPS, ABS, toughened PVC, rubber toughened PMMA (RTPMMA) and rubber-toughened epoxy are all rubber-toughened polymers that show tremendous ductility improvement by the inclusion of rubber particles. Fig. 1.7(b) shows an example of the rubber particle content on the stress-strain curve of RTPMMA. The ductility shown in Fig. 1.7(b) is maximum when the rubber content, w_p, is about 35%, above or below which the ductility is reduced.

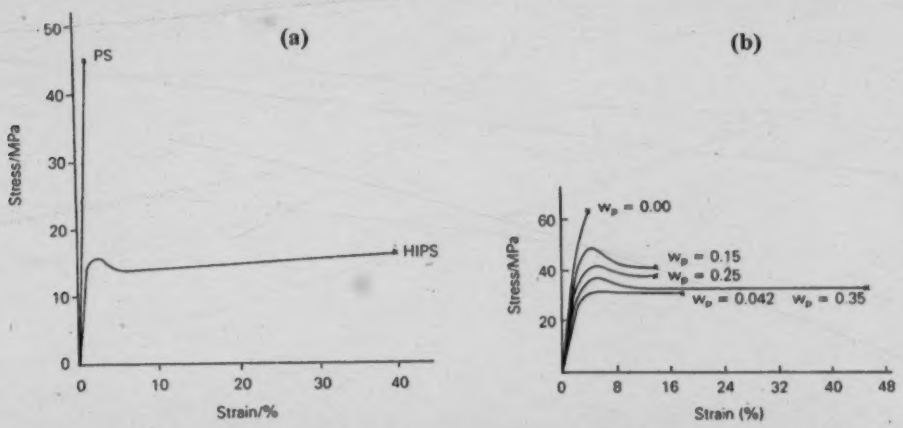

Fig. 1.7 Stress-strain curves for rubber-toughened polymers (Young and Lovell [36]). (a) Polystyrene (PS) and high-impact polystyrene (HIPS), and (b) Rubber-toughened poly(methyl methacrylate) showing the effect of the weight fraction of rubber particles, w_p.

1.3 ABS

ABS is a rubber-toughened polymer and has great market relevance. It is used from appliances to car parts because of its good properties balance. ABS, in fact, has a valuable compromise in mechanical, aesthetic and processing properties. It was the second rubber-toughened polymer manufactured commercially, after HIPS.

ABS consists of a matrix of random styrene-acrylonitrile (SAN) colopymer and a population of approximately spherical rubber particles. The rubber particles are generally made of polybutadiene (PB) and have sizes in a range from 0.05 to 5 μm. Uniform dispersion of rubber particles in the matrix is a key factor for effective toughness enhancement of ABS. Adhesion between the matrix and the rubber particle is through graft SAN-PB copolymer that provides strong bonding at the interface. The basic structure of ABS is shown in Fig. 1.8. The presence of rubber particles is the reason for the improved toughness of ABS [37,38]. The matrix, SAN, is in fact a quite brittle

material, whose critical stress intensity factor, K_c, is not far from that of polystyrene (PS), approximately 1.0~1.2 MPa·m$^{1/2}$. Emulsion polymerization and bulk polymerization are the standard methods of synthesizing ABS polymers.

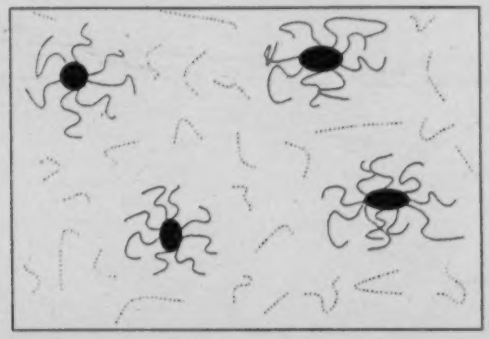

Fig. 1.8 A graphical representation of the basic structure of ABS (Lee [39])
(Spheres: block polymer of butadiene; solid lines: grafted random copolymers of styrene and acrylonitrile; dotted lines: free random copolymers of styrene and acrylonitrile)

ABS exhibits similar, but not identical stress-strain behavior to HIPS. For ABS, stress-whitening and shear yielding are followed by localized necking. The neck becomes intensely white, and the specimen breaks at a lower strain than comparable HIPS, because the stress is increased in the neck region. A typical stress-strain behavior of ABS is depicted in Fig 1.9.

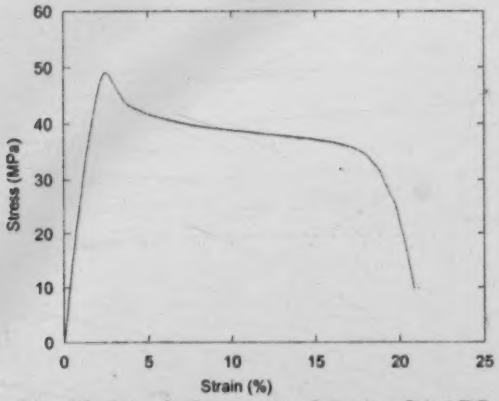

Fig. 1.9 A typical stress-strain curve for ABS

1.4 Deformation and fracture of polymers

There are two types of bonds governing the mechanical response in polymers: the covalent bonds between atoms and the secondary van der Waals forces between molecular segments. Ultimate fracture normally requires breakage of the former, but the secondary bonds also play a major role in the deformation mechanisms that lead to fracture.

Two modes of plastic deformation are common in polymers: shear yielding and crazing. For shear yielding, molecules slide with respect to one another when subjected to a critical shear stress. This occurs at constant volume and can take place uniformly throughout the sample under tensile or compressive loading. Shear yielding criteria can be based on maximum shear stress (Tresca criterion) or octahedral shear stress (von Mises criterion).

Certain polymers, particularly thermoplastics in the glassy state, are capable of undergoing localized plastic deformation, known as crazing. This was found to take place only when an overall hydrostatic tensile stress exists. Crazing occurs typically at about one-half of the yield stress of the polymer. Its occurrence does not usually cause any detectable change in slope of the stress-strain curve, but causes the material to undergo an increase in volume. On the macroscopic level, crazing appears as a stress-whitened region, due to the change of refractive index. The craze zone usually forms in a direction perpendicular to the maximum principal stress. Closer examination shows that crazes consist of aligned packets called fibrils. Micro-voids form between the fibrils. The aligned structure enables the fibrils to carry very high stresses relative to the undeformed amorphous state because covalent bonds are much stronger and stiffer than the secondary

van der Waals bonds.

Crazing and shear yielding are two competing mechanisms; the dominant mechanism for a polymer depends on molecular structure, stress state and temperature. A large hydrostatic tensile component is conducive to crazing, while a large deviatoric stress component is in favor of shear yielding.

The two mechanisms can occur simultaneously in most rubber-toughened polymers [40]. Differences in the contribution of the two mechanisms to the overall deformation cause the differences in tensile behavior between HIPS and ABS. In HIPS, crazing dominates with little evidence of shear yielding. Therefore, HIPS does not show necking but only stress whitening. In ABS, on the other hand, crazing and shear yielding proceed simultaneously, so that the specimen exhibits both stress-whitening and necking.

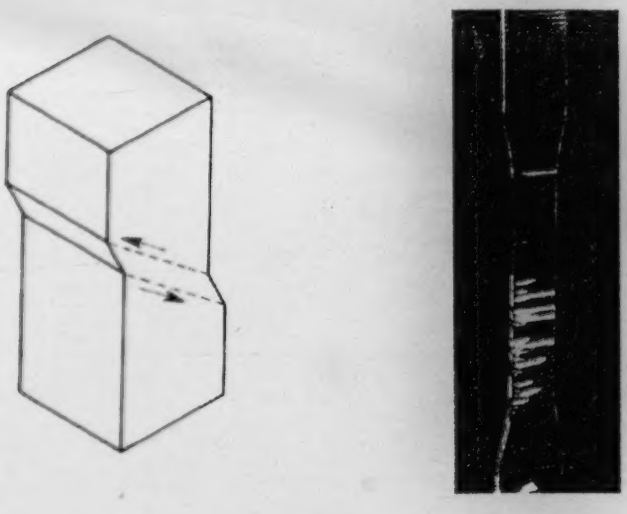

(a) (b)

Fig. 1.10 (a) Shear yielding under tension (Bucknall [54]), and (b) Sample of polycarbonate containing several crazes (Young and Lovell [36])

1.5 Biaxial tests

Many biaxial tests designed in the past used tubular specimens, to take advantage of a uniform stress field and versatility in varying the stress fields, as the stresses are generated through an axial force, torsional moment and internal pressure that can be adjusted independently. However, this method has the disadvantages in that the stress is not completely uniform over the thickness, and that the surface of the specimen is curved. Also, the material for the test has to be available in a tubular form with a relatively thin wall. In some cases, end-pressure-sealing is also a problem.

In view of the problems for the tubular specimens, Mönch and Galster [41] proposed a cruciform type flat specimen (Fig. 1.11(a)) of uniform thickness that produces a uniform stress state inside the central square of the specimen. In order to study the stress distribution, photoelastic models made of 10mm thick Araldit B were tested and were found to have a deviation from uniform stress of less than 1.4% (Fig 1.11(b)).

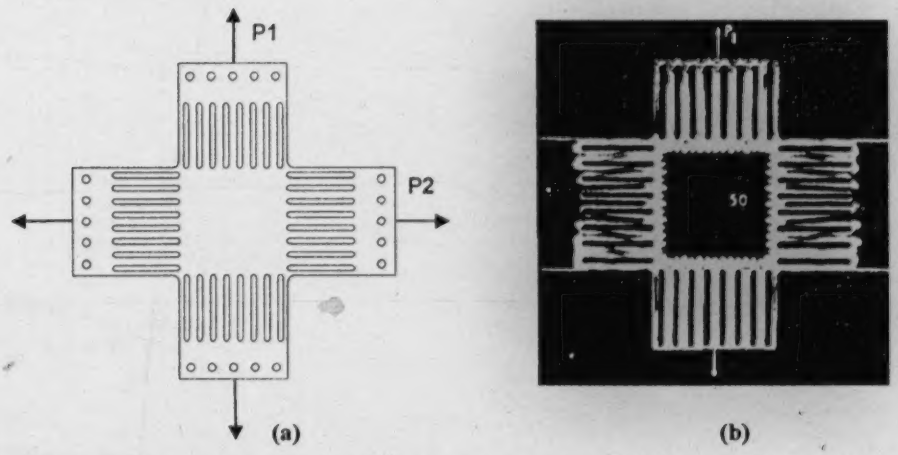

Fig. 1.11 (a) Specimen and (b) its fringe pattern under uniaxial force (Mönch and Galster [41]).

Using cruciform specimens, Cridland and Wood [42] also investigated three kinds

of designs to increase the field of uniform hydrostatic tension. They used isochromatic pattern to predict the stress distribution and concluded that a shape similar to the specimen proposed by Mönch and Galster showed reduced stress concentration and increased isotropic region, covering virtually the whole central square. They also made the triaxial test specimen based on this model using Calestone (a dental plaster) and did the triaxial hydrostatic test. Their test apparatus applies three pairs of opposing forces of equal magnitude in the 3 orthogonal directions. The test results showed that the hydrostatic stress required to produce the failure was about 50% higher than the ultimate tensile strength of Calestone under uniaxial stress.

Joshi and Shewchuk [43] investigated the effect of biaxiality of stress on the fatigue-crack-propagation rate in aluminum alloy. Round and elliptical plates, simply supported at the edges, were subjected to bulge bending. The nominal stress-biaxiality ratios (ratio of 1^{st} principal stress to 2^{nd} principal) of 1:1, 1:0.86, and 1:0.75 were obtained in the plane of the specimen. They concluded that for a given number of cycles, increasing the transverse stress decreases the toughness, in terms of crack growth rate and crack size development.

The photoelastic model of Mönch and Galster's specimen showed that for a 6.25 x 6.25 *inch* square plate a uniformly stressed 4.70 x 4.70 *inch* square could be achieved, but it also showed higher order fringes around the loading points which are indications of high stress concentration. Hayhurst [44] overcame the problem of high stress concentration by uniformly thinning the central region from 0.25 *inch* to 0.19 *inch* in thickness so that the uniform central stress exceeds the largest stress at the loading points. He also used aluminum alloy specimens to study creep rupture behavior by loading the

specimen in a deadweight loading system. The rupture time of the aluminum-alloy plates when subjected to biaxial tensile stress was found to be significantly less than that in uniaxial tests carried out under the same tensile stress values, suggesting that the alloy's fracture toughness was reduced under biaxial loading.

Kelly [45] used the similar shape of cruciform specimens to Hayhurst's to investigate the creep in copper. Thickness of the gauge section was reduced from 13mm to 6mm, and six slots were introduced in each arm, strips between which transmitted tension in the direction of the slots and also deflected as cantilevers to reduce constraint on the gauge area in the direction normal to the slots, as shown in Fig. 1.12. His specimens were loaded by large cast iron weights and only static loading was applied. The test results showed that the creep strain generated under equi-biaxial tension was approximately one half of the strain under uniaxial tension. Therefore, it can be concluded that the transverse stress decreased the creep rate and increased the toughness in creep. His result was contradictory to Hayhurst's even though their specimens had the similar shapes.

Hopper and Miller [46] did two series of tests on a high strength aluminum alloy. The first series examined fatigue crack propagation under different biaxial stresses in non-notched plate specimens. (note: the specimens had a "crack" not a "notch", following the definition given in the paper). The second series used specimens containing a central circular "notch", and crack growth rates under the biaxial stress states were again determined. Since his testing equipment could not apply cyclic loading simultaneously in two directions, load in one direction was kept constant. Results from both series of tests showed that additional compressive transverse load gave higher crack growth rates and

opposite was found for the tensile load.

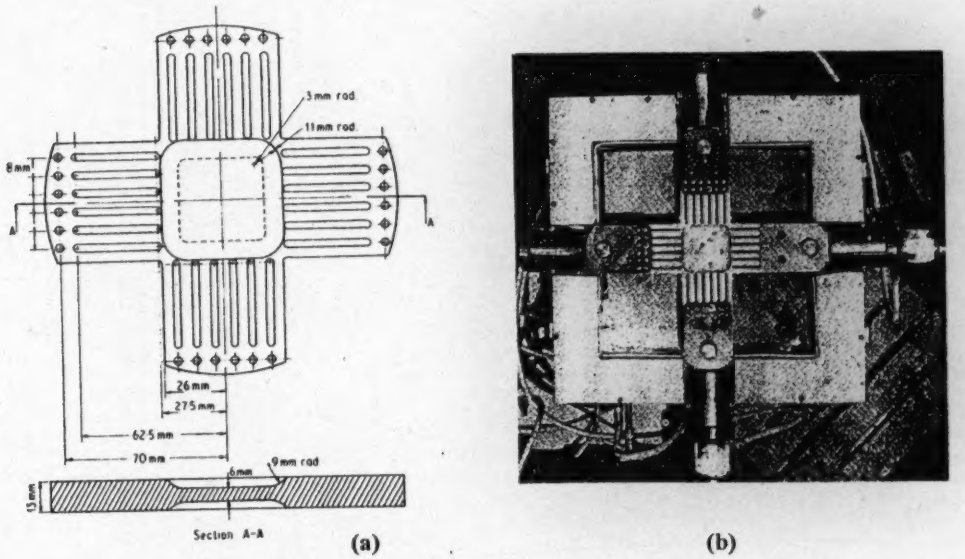

Fig. 1.12 (a) Specimen, and (b) test equipment used (Kelly [45]).

Kitagawa and Yuuki [47] derived the polynomial of stress intensity factor (K_I) and compared the numerical result with FEM. They investigated the fatigue crack growth behavior of structural steel cruciform specimens using a four-axis servo hydraulic fatigue testing machine. The result suggested that:

i) A static load parallel to a crack has no effect on the fatigue crack growth rate, whereas a cyclic load parallel to a crack does have an effect.

ii) When the cyclic loads in the two directions are synchronized, the fatigue crack growth rate decreases with the increase of the transverse cyclic load amplitude that is applied in the direction parallel to the crack.

iii) The fatigue crack growth rate increases with the increase of phase difference from 0 to π for equi-biaxial loading conditions.

Therefore, it can be concluded from their study that the transverse cyclic stress increased the toughness.

Hoshide et al. [48] conducted fatigue crack propagation tests under conditions of equi-biaxial, uniaxial and shear loading, using cruciform specimens of structural carbon steel in a servo hydraulic testing machine. Their test results suggested that the fatigue crack propagation rate was decreasing in the order of uniaxial, equibiaxial, and shear loading. Therefore, the transverse stress was concluded to increase the toughness.

The studies mentioned so far were on metals. There are a few studies of the effect of biaxial loading on the toughness of polymers and one of them was made by Leevers et al. [49]. They modified the previous biaxial specimens to study the crack growth rate under biaxial tension. The specimen used had a pre-crack of 30mm in length and was made of PMMA with uniform thickness of 6.5mm and PVC of 3 and 6 mm thick. The testing machine used had a single hydraulic actuator to apply in-phase tensile loads to both. The test results showed that the effects of stress biaxiality on crack propagation rates in PVC was almost absent. In PMMA, however, the transverse stress reduced crack growth rate and slightly increased fracture toughness.

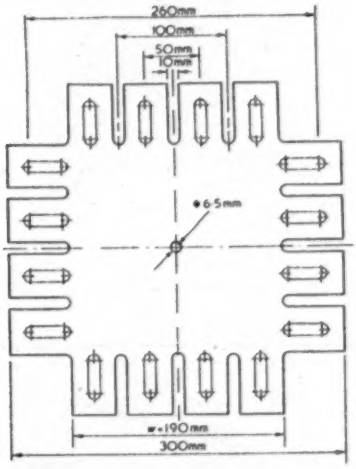

Fig. 1.13 Cruciform specimen (Leevers et al [49]).

Atkins et al.[9] used ABS and PVC sheets to make cruciform specimens (Fig. 1.14(a)) for both monotonic and fatigue fracture tests. They used a simple rig (Fig. 1.14(b)) on a uniaxial testing machine to achieve the biaxial loading. They measured the essential work (section 1.1.5) for the various biaxialities and investigated the effect of transverse loading on the toughness variation. Their test results show that monotonic toughness is least in equi-biaxial tension while it is greatest in uni-axial tension. On the other hand, fatigue crack growth rates decreased as the load parallel to the ligament increased. In terms of Paris plots [50,51], n in $(da/dN) = C(\Delta K)^n$ was found to be more or less unaffected by the biaxial stress state, but C decreased with the increase of the transverse stress. Therefore their results showed the decrease of toughness with the introduction of transverse stress under monotonic loading while the increase of toughness with introduction of the transverse stress under fatigue loading.

As a general conclusion from the past research work, the effect of biaxial stress on the toughness was not consistent. Some researchers showed that the transverse stress

increased the toughness, such as in static creep tests, cyclic fatigue tests and in monotonic fracture tests. However, other researchers showed contradictory results. Moreover, the materials used for biaxial tests in the past were mainly metallic materials such as copper, aluminum and steels. Little work has been done on rubber-toughened polymers.

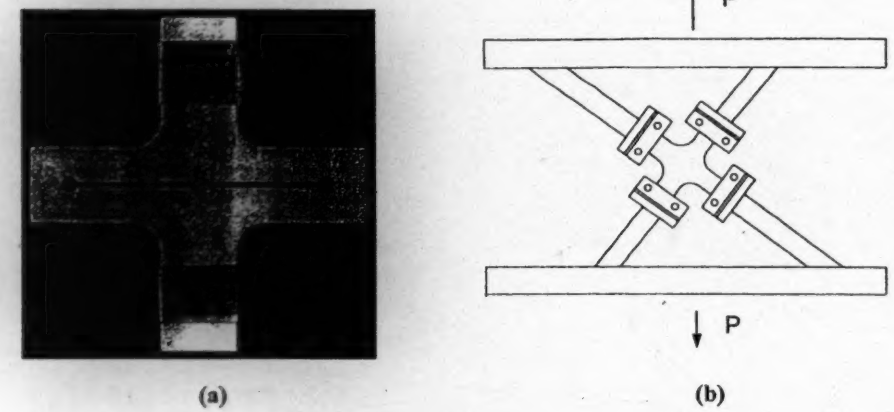

Fig. 1.14 (a) Specimen, and (b) test equipment (Atkins et al [9]).

2. Test Methodology

The test program consists of three parts: uniaxial fatigue, biaxial fatigue and monotonic tensile tests. The two fatigue tests were to introduce potential damages that might be caused by the fatigue loading but before any visible cracks were initiated. Since the published literature is yet to show the existence of a threshold fatigue loading or a critical number of cyclic loading above which significant toughness drop occurs, but without any visible cracks or damages, this test program was designed to search for the threshold loading level and the corresponding loading cycles for ABS that are critical for such a toughness change. Evaluation of the toughness change was through the monotonic tensile test using standard dog-bone specimens.

A summary of the test procedures is given in Fig. 2.1, that shows the use of rectangular strip specimens and cruciform specimens for uniaxial and biaxial fatigue tests, respectively. The fatigue-loaded strip and cruciform specimens were then machined to dog-bone shape for the monotonic tensile tests for the toughness evaluation. This procedure removed the edge surfaces of the strip specimens that are known to be prone to damage initiation. Preliminary tests have been conducted to ensure that the dog-bone specimens machined from the fatigued strip specimens contained no damage from the edges, and had the same surface condition as that machined from the cruciform specimens. Details of the test procedures and condition are described in the following

section.

Stress distribution in the cruciform specimens was analyzed by the finite element method (FEM) using a commercial code ANSYS R7.0. The FEM analysis enabled us to estimate the stress level and the biaxiality of the fatigue loading that had been applied to each of the dog-bone specimens during the biaxial fatigue loading, which is needed to evaluate the effect of the biaxial fatigue loading on the toughness drop.

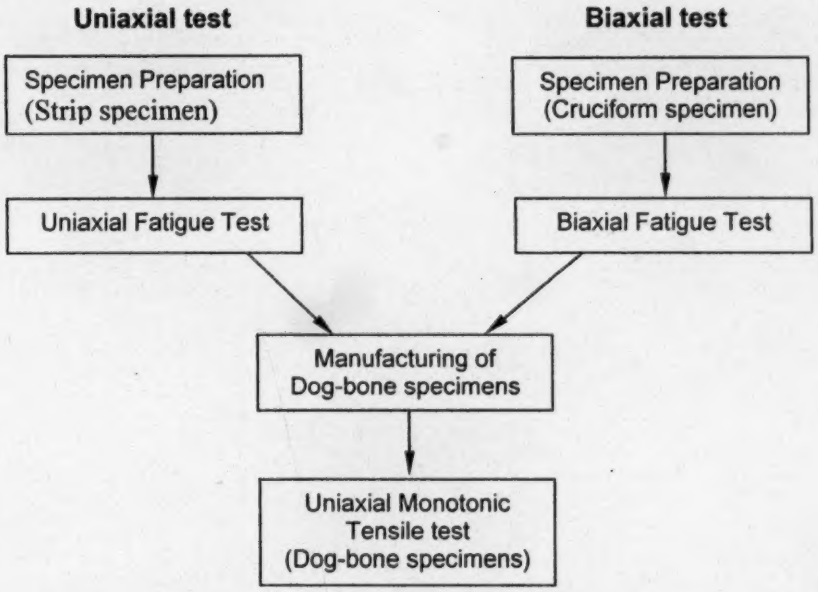

Fig. 2.1 Procedure for toughness evaluation under uniaxial and biaxial fatigue loadings.

2.1 Uniaxial fatigue test

2.1.1 Test specimens

Extruded ABS plates of 300x300mm^2 and nominal thickness of 3.2mm were provided by Denki Kagaku Kogyo Co. Ltd., Japan. Tensile tests were conducted to

ensure that the extrusion process did not introduce any molecular orientation that may have affected the isotropy of mechanical properties. Both results showed the same tensile strength (50MPa) and Young's Modulus (2500MPa) and this material could be regarded as isotropic.

Strip specimens were machined from the plates for the uniaxial fatigue test, after which dog-bone specimens were machined from the strip specimens to remove the potentially damaged side edges so that the specimens for the tensile test were free from edge cracks or crazes. The level of fatigue loading was determined based on the cross sectional area of the strip specimen.

2.1.2 Procedure for the specimen preparation

For the fatigue tests, strips of 25x145 mm^2 were cut from the ABS plates along 0°, 45° and 90° with respect to the rolling direction, though the preliminary tests described above had confirmed that no orientation effect existed in these plates. These strips were milled to 19mm wide and 136 mm long, and the machined edges were then polished with 400 and 600 grit wet sand papers. Surface across the width of the ABS strips was not machined, nor polished. These strip specimens were handled with extreme care to ensure that no scratches were introduced during the machining.

2.1.3 Fatigue tests

Uniaxial and biaxial fatigue tests were conducted using the same hydraulic testing machine, MTS Series 812, with a 10,000lb load cell (Fig. 2.2). Fatigue frequency was 0.1 Hz and the full load range used was 1,000 lb, i.e. 10% of the load cell capacity.

Loading functions of "Haver" sine wave, from 0 to a pre-determined force level, were applied under a load-control mode. In the rest of the thesis, the peak forces used for the fatigue tests were referred to in terms of the percentage of the tensile yield strength (50MPa), that is 30%, 40%, 50%, and 60% for applied stresses of 15MPa, 20MPa, 25MPa and 30MPa, respectively.

Due to limited availability of the testing machine, we used relatively high percentage of yield strength for the fatigue loading to minimize the time required for the fatigue tests. For the range of fatigue loading used in the study, 500 cycles were found to be sufficient to detect the toughness change in the above range of fatigue loading, as to be shown in Chapter 3. It should be noted that at a loading level above 30MPa (60% of the yield strength), fracture occurred or visible cracks were generated before 500 cycles were reached, thus not suitable for this study, as this study focused on the toughness variation before any crack initiation. More than 15 specimens were tested for each of the loading conditions.

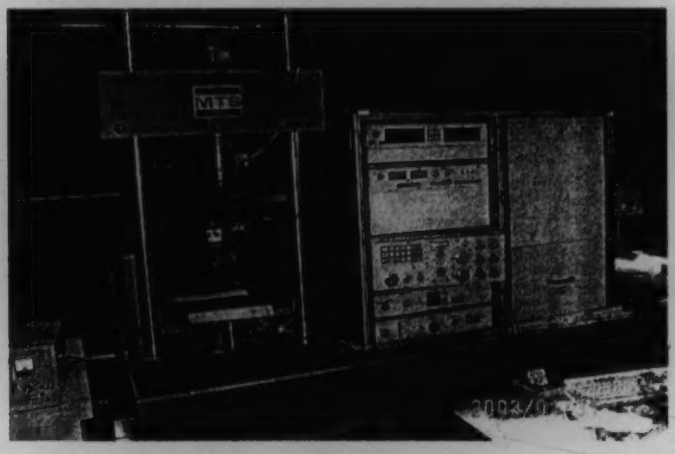

Fig. 2.2 10,000 lbf MTS machine, series 812

2.2 Biaxial fatigue test

2.2.1 Test rig

Biaxial test rig used in this study is shown in Fig. 2.3, and its design drawing in Fig. 2.4. The test rig was mounted on the 10,000 lbf MTS machine that was used in the uniaxial fatigue test, as shown in Fig 2.3. The base plate of the test rig was fixed on the shaft attached to the hydraulic cylinder and was moved up and down during the fatigue loading. The grippers, indicated in Fig. 2.4, grip all four arms of the cruciform specimen of which geometry and dimensions are to be given in the next section. The vertical movement of the base plate was transmitted to the grippers by connecting rods that the grippers moved horizontally along the slide rails, applying tensile forces to the specimen. Forces applied by the four grippers were evened by using the adjusting bolts on which strain gauges were attached to measure the forces applied to each arms, as shown in Fig. 2.4. The test rig was attached to the MTS load cell through connecting rods. Therefore, once the forces applied by the grippers were evened, the force values read by the MTS load cell could be used to control the cyclic strokes of the test machine.

Each of the four grippers was tightened using 2 bolts. Care was taken so that the grippers were tightened in an even fashion, to avoid the specimen warping due to asymmetric forces applied through the grippers. If the forces detected by the strain gauges implanted to the each axis were not balanced after the tightening process, it was relieved through turning the adjusting bolts to increase or decrease tensile force applied on each arm of the cruciform specimen.

Fig. 2.3 4-axis biaxial test rig

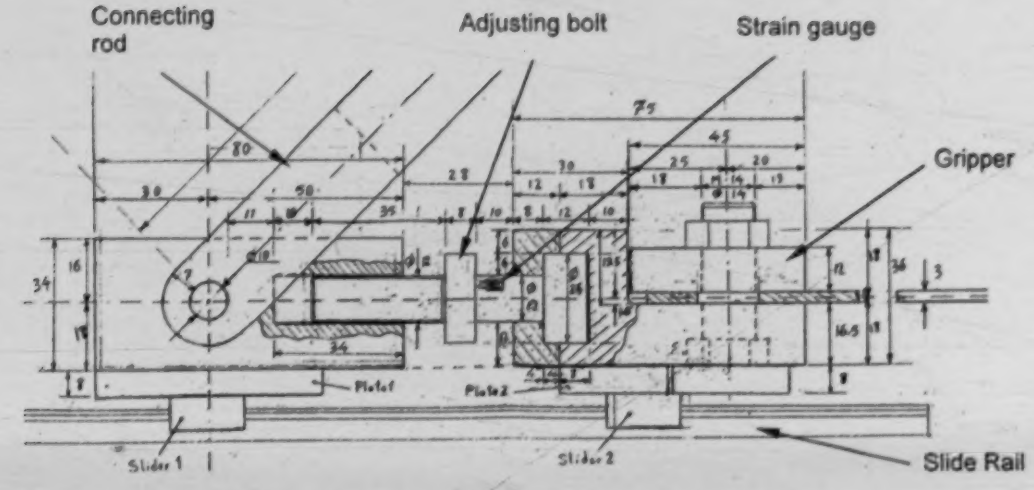

Fig. 2.4 Front view of the design drawing of the biaxial test rig

2.2.2 Design of test specimens

Cruciform type specimens (Fig. 2.5) were used for the biaxial fatigue test. Previous biaxial work reported in the literature[32,35,36], as discussed in section 1.5, used cruciform specimens with slots in the arms to provide flexibility so that the specimen arms do not transmit any shear force. However, the materials used for the slotted specimens were metal-based that have much better ductility and toughness than ABS. For ABS, the stress concentration occurring around the end corner of the slots leads to premature fracture during the fatigue test. Without the slots, as shown in Fig. 2.5, the FEM analysis in chapter 3 estimated that the shear stress values were less than 10% of the 1st principal stress, that is, below 2.5MPa at the central part where the 1st principal stress was 25MPa. Therefore, the shear stress component can be ignored for our test and the non-slotted specimen geometry as shown in Fig. 2.5 was adopted.

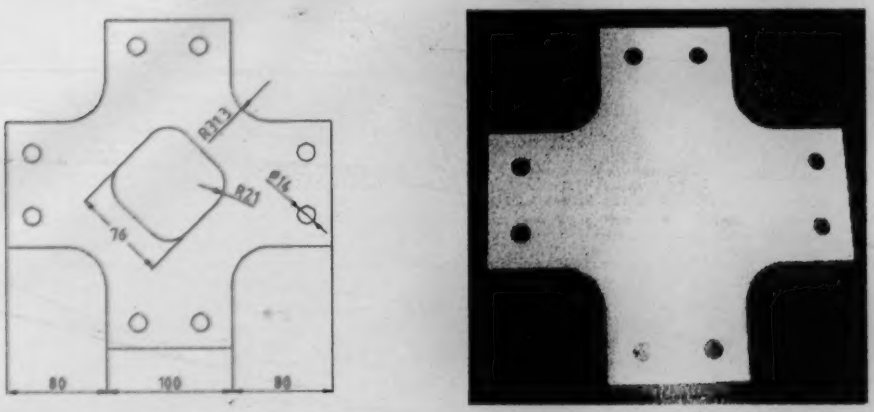

(a) (b)

Fig. 2.5 Cruciform specimen: (a) the dimension, including thickness reduction in the centre, and (b) a photograph of a machined specimen

Preliminary test results showed that the maximum stress level achievable in the central region was limited by the stress concentration along the round corner. The only way to raise the stress level in the central part is to lower the stress concentration along the round corner. FEM modeling suggests that the stress concentration was lowered by increasing the radius of the round corner. Based on the availability of the machine tools, we have determined the radius of the round corner to be 31.3 mm.

2.2.3 Procedure for the specimen preparation

The ABS plates were cut and milled to the cruciform geometry. Drilling jig and milling jig (Fig. 2.6) were made as templates for the machining. The machined surfaces around the corners were then polished using 400 and 600 grit wet sand paper.

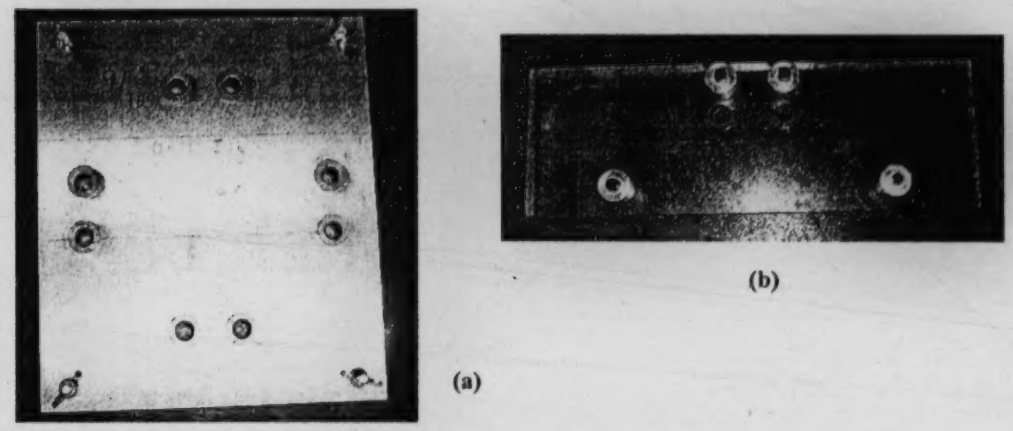

Fig. 2.6 (a) Drilling jig, and (b) milling jig for cruciform specimen.

2.2.4 Load cell calibration

Tensile force along each axis of the cruciform specimen was measured using a tubular load cell to ensure that a desired stress level was provided. The load cells are part

of the adjusting bolt (Fig. 2.4) that has strain gauges attached to measure the force applied by the biaxial test rig. Load-strain relationship was calibrated for each adjusting bolt before assembling the test rig. The calibration curve was quite linear with the correlation coefficient, R, above 0.999, and the load measurement showed excellent repeatability. However, the adjusting bolts were also undergoing fatigue loading during the test, and the load-strain characteristic curve may have changed. It is therefore necessary to check the accuracy of the strain gauge signals and re-calibrate the load-strain curve regularly, after the test rig was assembled.

The above process to calibrate the load-strain curve for each adjusting bolt cannot be carried out without dissembling the gripper, but dissembling and re-assembling are very time-consuming and tedious processes. To avoid those processes, a dog-bone type calibrator (Fig. 2.7) was manufactured for this purpose. The calibrator is a dog-bone-shaped aluminum specimen with two strain gauges embedded in the gauge section. The calibrator can be loaded on the test rig in the same way as the cruciform specimen, to calibrate two opposite axes of the rig each time. Since the calibrator does not provide absolute calibration for the load cells, the gripper need to be dissembled on a regular basis, to calibrate the load-strain relationship for each adjusting bolt.

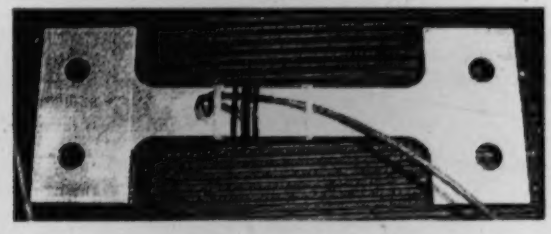

Fig. 2.7 Dog-bone calibrator

2.2.5 Fatigue test

The tensile force applied through each axis of the cruciform specimen, which was required to apply the desired stress level in the central region, was estimated using FEM analysis. The fatigue tests were then conducted in a closed-loop force control mode, using signals obtained from the MTS load cell. Force applied through one of the 4 axes was monitored through the whole testing period to ensure that the loading condition did not change during the test.

The stress levels for the biaxial fatigue testing were the same as those for the uniaxial fatigue testing. The fatigue frequency was 0.1 Hz. The biaxial stress levels, in terms of the percentage of the tensile yield strength (50MPa), of 30%, 40%, 50%, and 60% were used for the biaxial fatigue tests. Ratio of biaxial forces was 1 to 1 unless indicated otherwise.

2.3 Tensile test

As mentioned section 1.1, toughness can be defined as the total work to fracture, that is, the energy absorbed before fracture. For specimens with no pre-existing cracks, the energy absorbed is quantified by the area under the stress-strain curve of a pure tensile test. Tensile tests were conducted to obtain the stress-strain curve of the specimens after the fatigue loading.

2.3.1 Test specimens

Dog-bone specimens (Fig. 2.8) were machined from strip specimens after the uniaxial fatigue tests and from cruciform specimens after the biaxial fatigue tests. The

width and length in the gauge section of the dog-bone specimens are 10 mm and 30 mm, respectively. The neck region was made with a radius of 31.3mm that is the largest radius achievable using the existing the machining tools.

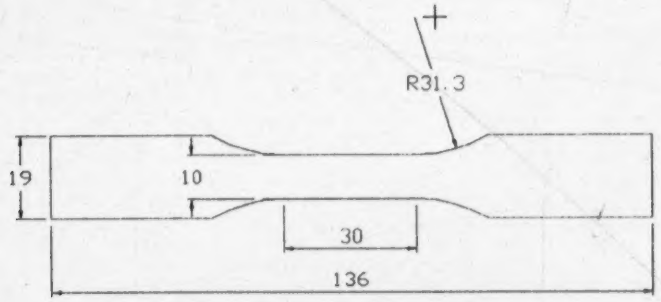

Fig. 2.8 Dog-bone type tensile test specimen

2.3.2 Specimen preparation

The cutting plans to make the dog-bone specimens out of cruciform and strip specimens are shown in Fig. 2.9. The cruciform specimens were cut to strips first, using a band saw, to dimensions similar to those of strip specimens for uniaxial fatigue test. These strips were then milled to dog-bone specimens using the milling jig shown in Fig. 2.10. Care was taken to make sure that the dog-bone specimens from the cruciform specimens and those from uniaxial strip specimens maintained the oroginal surface finish.

To ensure that the tensile fracture occurs in the gauge section, a polishing jig (Fig. 2.10 (b)) was used to reduce central part of the gauge section by 0.1mm (1% of the width), following the recommendation in ASTM D638. The width reduction was achieved through hand polishing using 400 and 600 grit wet sand papers. The use of the polishing jig ensured the consistency of the dimensional reduction.

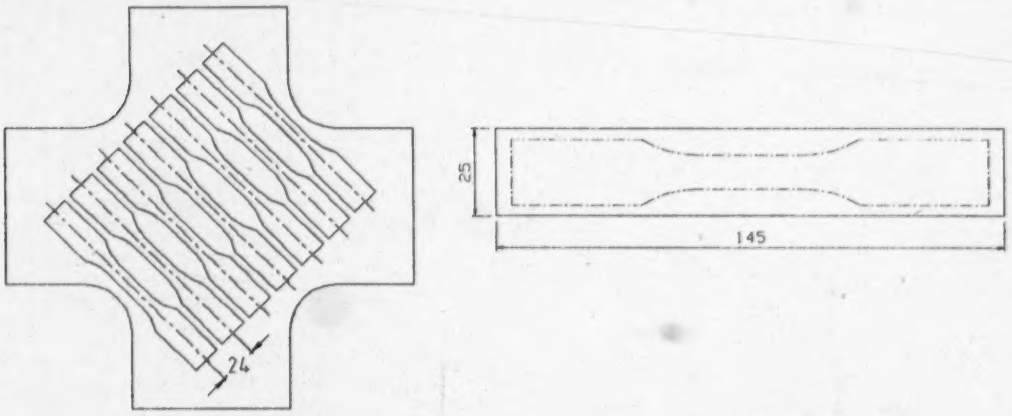

(a) (b)

Fig. 2.9 Cutting plan of (a) cruciform specimen, and (b) strip specimen.

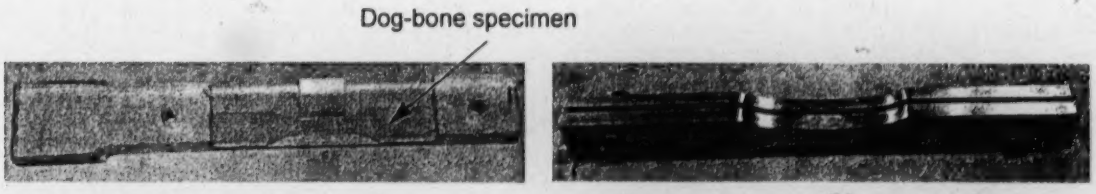

(a) (b)

Fig. 2.10 (a) Milling jig with specimen, and (b) Polishing jig for width reduction in the gauge section.

2.3.3 Tensile test

A universal screw-driven testing machine from Instron was used for the tensile test, at the ram speed of 0.2 *inch/min* (5*mm/min*), conforming to the range of testing speed specified in ASTM D638. The deformation was measured using an extensometer with the initial gauge length of 1 *inch* (25.4*mm*).

3. FEM Modeling

3.1 FEM model

The geometry of the cruciform specimen and its stress distribution were analyzed using ANSYS R7.0. Due to central symmetry of the geometry, the FEM model is only a quarter of the specimen. Elements of 8 nodes (Plane 82) were adopted, with the assumption that no slippage occurred between the gripper plate and the specimen. As a result, modulus of the gripper material (steel) was assigned to the area covered by the gripper plate. The elastic material properties of ABS used in this study were known from the preliminary tests:

Young's modulus (E) = 2500MPa

Poission's ratio (ν) = 0.35

Thickness (t) = 3.2mm

The elastic material properties of steel are:

Young's modulus (E) = 206.8GPa

Poission's ratio (ν) = 0.31

Thickness (t) = 35mm

The FEM model of a quarter of a specimen is shown in Fig. 3.1. The normal displacements along the symmetric lines with x=0 and y=0 were assumed to be zero and

the surface loads were assigned to each end of the grippers.

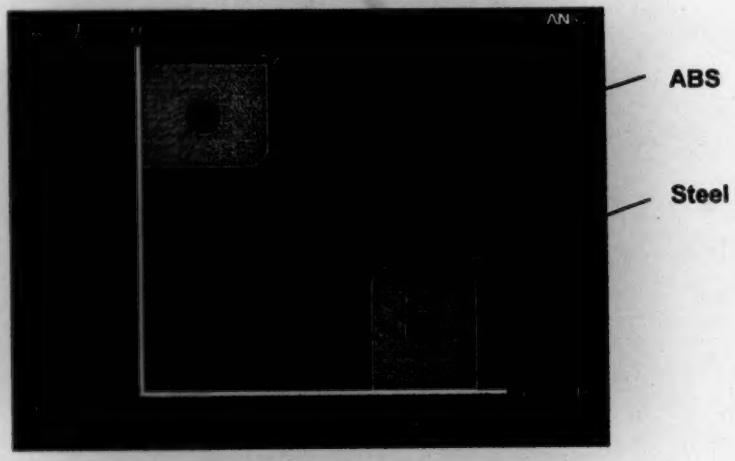

Fig. 3.1 FEM model of a quarter of specimen

3.2 Stress analysis with original thickness

One of the purposes of the FEM analysis is to find the geometry to raise the stress in the middle area to 25MPa (50% of the yield strength) and minimize the stress concentration along the round edge. The distribution of the 1st principal stress (S1) for the geometry in Fig. 2.5 is indicated with the variation of the color in Fig. 3.2 where the color changes from blue to red with the increase of 1st principal stress. Stress concentration occurs along the round corner; however the highest stress does not occur in the middle of the corner. As shown in Fig. 3.2, the highest stress indicated with red color occurs at points deviated from the midway of the corner.

Fig. 3.3 compares the 1st and 2nd principal stresses along the stress path in Fig. 3.2. The minimum 1st principal stress (S1) is 15MPa at the center and it increases as the position moves away from the center while the 2nd principal stress (S2) is the same value as S1 at the center and continually drops to zero at the edge. A nominal stress ratio of 1 to

1, corresponding to an equi-biaxial stress state, is achieved within a central region with a radius of 30mm. In this region, the maximum variation of 1st and 2nd principal stresses with respect to the stress at the center is within 6.7%.

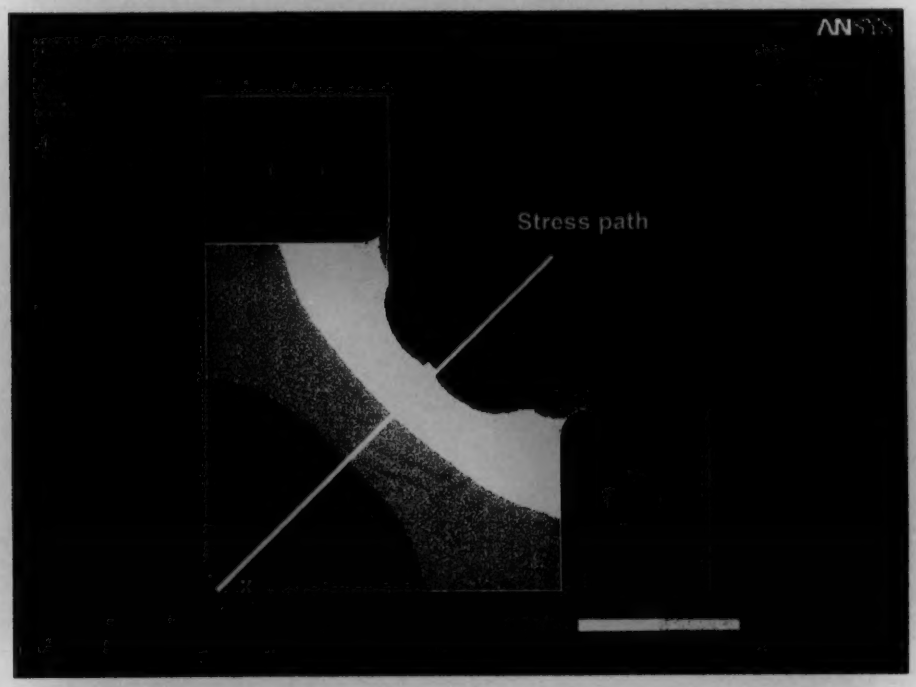

Fig. 3.2 FEM contour plot showing the distribution of the 1st principal stress in the cruciform specimen under equi-biaxial loading

Since the stress levels used in uniaxial fatigue tests are 15MPa, 20MPa, 25MPa, and 30MPa (section 2.1.3), it is wanted to subject the cruciform specimens to the same stress levels in both directions in the central region. However, as shown in Fig. 3.3, when the biaxial stress in the central region reaches 15MPa, the stress at the round corner is already 33MPa. From the preliminary test, the maximum allowable stress to avoid fracture within 500 cycles of fatigue loading is 35MPa and the maximum stress of this geometry at the round corner is very close to the maximum allowable fatigue stress. If the

stress at the center is raised to 25MPa which is 50% of yield strength (50MPa), the maximum stress at the round corner will reache 55MPa which is even higher than the yield strength. We found that it is impossible to raise the stress at the center higher than 18MPa with any variation of the dimension by maintaining constant thickness.

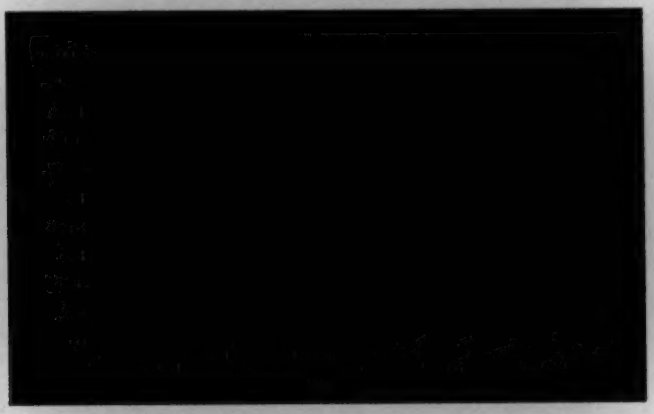

Fig. 3.3 Stress variation along the stress path given in Fig. 3.2

3.3 Stress analysis with reduced thickness

From the above analysis, it is concluded that specimen thickness should be modified to raise the biaxial stress in the central region without the stress exceeding 35MPa at the round corner. Cruciform specimen with reduced thickness in the central region is shown in Fig. 3.4 and the stress variation along the path in Fig. 3.4 is given in Fig. 3.5. Fig. 3.5(a) shows the stress with the thickness reduction to 60% (1.92mm) of the original thickness (3.2mm). This raised equi-biaxial stress to 21.3MPa in the central region, with the maximum stress in the round corner reaching 35MPa. Further reduction of the thickness to 40% (1.28mm) of the original thickness generates equi-biaxial stress of 25MPa in the central region with the maximum stress around the corner only slightly

over 35MPa, as shown in Fig. 3.5(b). It should be noted that the highest value of 1st principal stress (S1) in Fig. 3.5 is not the highest stress occurring in the specimen. As shown in Fig. 3.2, the point where the highest stress occurs is not along the path given in Fig. 3.4. Since further thickness reduction would make the specimen too fragile to handle, the thickness reduction up to 40% (1.28mm) was adopted in this study. The achievable equi-biaxial stress at the center was 25MPa with the maximum thickness reduction. Fig. 3.6 is a part of the cross-sectional view showing thickness reduction.

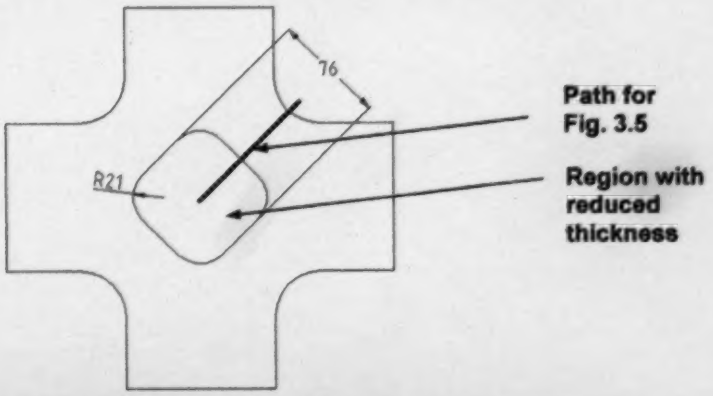

Fig. 3.4 Plan for thickness reduction in cruciform specimen (unit: mm)

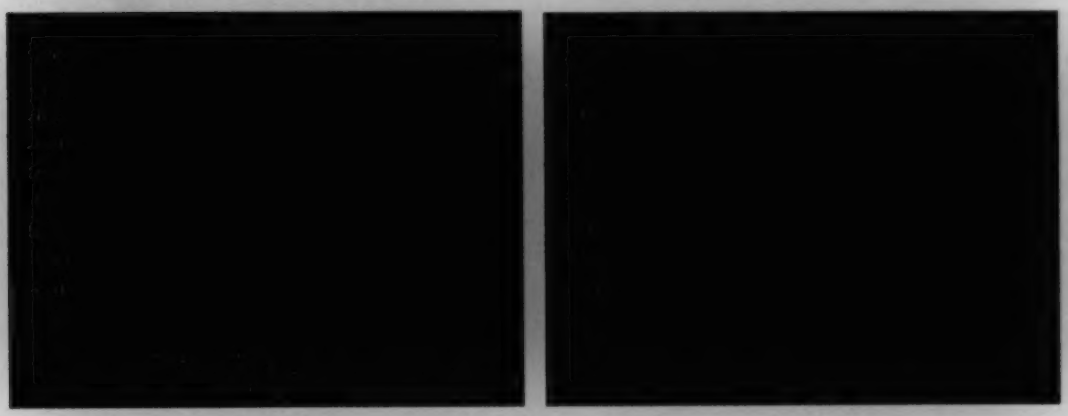

(a) **(b)**

Fig. 3.5 FEM results showing the 1st and 2nd principal stresses along the path given in Fig. 3.4. (a) with the thickness reduction to 1.92 mm (60%), and (b) with the thickness reduction to 1.28 mm (40%)

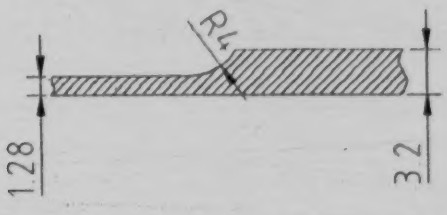

Fig. 3.6 Cross-sectional view of reduced thickness (unit: mm)

As shown in Fig. 3.5(b), the stress state inside the region with reduced thickness can be regarded as uniform equi-biaxial because the variation of the 1st principal stress and the 2nd principal stress from the stress at the center is within 5%. Three tensile test specimens (No. 3~5 in Fig. 3.7) could be made from this region and they were assumed to experience the same fatigue stress condition. Four more specimens (No. 1, 2, 6 and 7) could be made from outside the thinned region, i.e. from the region with original thickness. The stress calculated from FEM varies across the width of the tensile specimens shown in Fig. 3.7; therefore, the stress at the middle gauge section of each specimen was regarded as the fatigue stress applied to that specimen. Based on the FEM analysis, the 1st and 2nd principal stresses of specimen No. 1 and 7 are 30MPa and 6MPa, respectively, while those of specimen No. 2 and 6 were 21MPa and 9.6MPa, respectively.

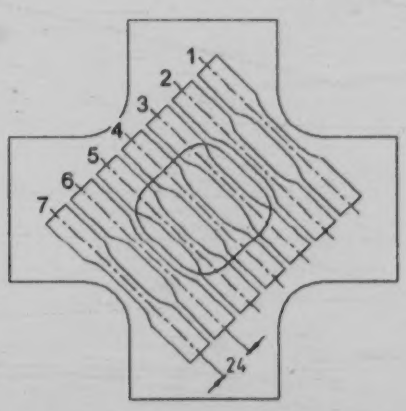

Fig. 3.7 Cutting plan of the cruciform specimen with reduced thickness

4. Effect of Fatigue Loading on Mechanical Properties

4.1 Introduction

As discussed in section 1.5, studies on metallic materials have not yet clarified whether the toughness increases under biaxial stresses, and less is known for polymers. Furthermore, none of the previous publications is concerned with the toughness change before any visible crack was initiated under uniaxial or biaxial fatigue loadings.

In this chapter, results on the toughness change of ABS specimens without any existing pre-crack, after 500 cycles of uniaxial or biaxial fatigue loading, will be discussed. The discussion will also include fractographic analysis of surfaces generated from the tensile tests that were used for the toughness measurement.

4.2 Cracking strain

All the toughness evaluation methods introduced in section 1.1 are used to determine the toughness for crack propagation, since most of the fracture tests have been conducted using specimens with a pre-crack. The results from pre-cracked specimens are not useful for characterizing the resistance to crack propagation that is known to be a significant part of total fatigue lifetime of a material.

We found an attractive measure to quantify the energy absorption capability of crack-free specimens, which can be used effectively to characterize how the fatigue loading affects the toughness. The measure is the strain at the on-set of final fracture, commonly known as fracture strain from tensile test, but named cracking strain here to note the difference in the specimens used for the tests. Representative stress-strain curves from tensile tests are shown in Fig. 4.1(a) from a non-fatigued specimen and Fig. 4.1(b) from a uniaxially fatigued specimen. The two figures show that the fatigue loading did not affect the mechanical properties such as yield strength or Young's modulus. The only change in the stress-strain curve is the cracking strain, that is, the strain at the on-set of fracture. As will be shown in this chapter, the two curves suggest that the cracking strain decreased about 30% after the fatigue loading, and is the only variation that affects the area under the stress-strain curve. Therefore, we conclude that the cracking strain can be used as a measure for the toughness change by the fatigue loading.

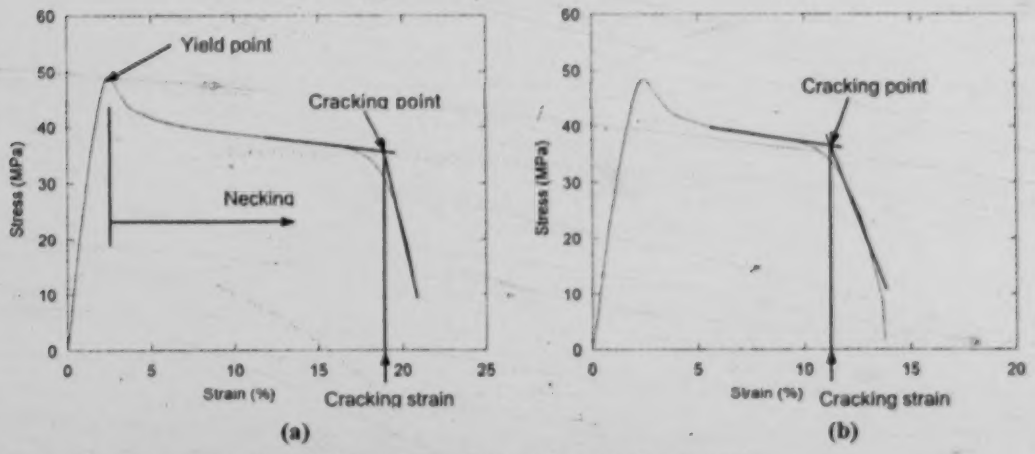

Fig. 4.1 Tensile stress-strain behaviors of non-fatigued and fatigued ABS.
(a) from a non-fatigued ABS specimen, and (b) from a fatigued ABS specimen (uniaxial fatigue loadings, 500 cycles, peak load at 20MPa)

4.3 Mechanical test results

Uniaxial Fatigue

The cracking strain values after various uniaxial fatigue loadings are summarized in Fig. 4.2. It should be noted that the very left point (◆ at 0MPa) is the cracking strain (or fracture strain) from the non-fatigued specimens. All the other specimens for Fig. 4.2 were under 500 cycles of specified fatigue stresses. In the case of uniaxial fatigue loading, as shown in Fig. 4.2 by the symbols of solid or open circles (● or ○), there was no toughness change up to the fatigue stress of 15MPa, above which a distinct drop of the cracking strain occurred, and the toughness drop leveled off above 25MPa. It should be noted that none of the specimens in Fig. 4.2 showed any visible crack or damage after the fatigue loading. The dashed line (- - - -) represents the trend of the toughness drop after the uniaxial fatigue loading, which clearly shows that the fatigue stress above the threshold value of 15MPa can significantly affect toughness of the ABS. Above 25MPa (about 50% of the yield strength), the cracking strain is reduced to less than 25% of the original value. The major toughness transition region lies between 15MPa and 25MPa.

It should be noted that at a fatigue stress level above 30MPa, stress whitening appeared around the specimen edge during 500 cycles, and the fatigue stress of 35MPa caused the specimen fracture before 500 cycles were reached. Therefore, 30MPa was very close to the maximum fatigue stress allowed for 500 cycles.

Uniaxial Fatigue with Reduced Thickness

The open circle (○) at 25MPa in Fig. 4.2 indicates the cracking strain of the uniaxially fatigued specimen with reduced thickness. It shows an apparent effect of

specimen thickness, that is, the specimens with reduced thickness showed a lower cracking strain than that for the specimens with the original thickness. This is believed to be the consequence of increased ratio of surface to volume. Chen et al. [52] reported the thickness effect on the ductility that the ductility increased with the decrease of the thickness up to the critical thickness determined by the maximum stress ratio (σ_{max}/σ_y), but the thickness in our study might be above the critical thickness and the ductility was not affected by the thickness.

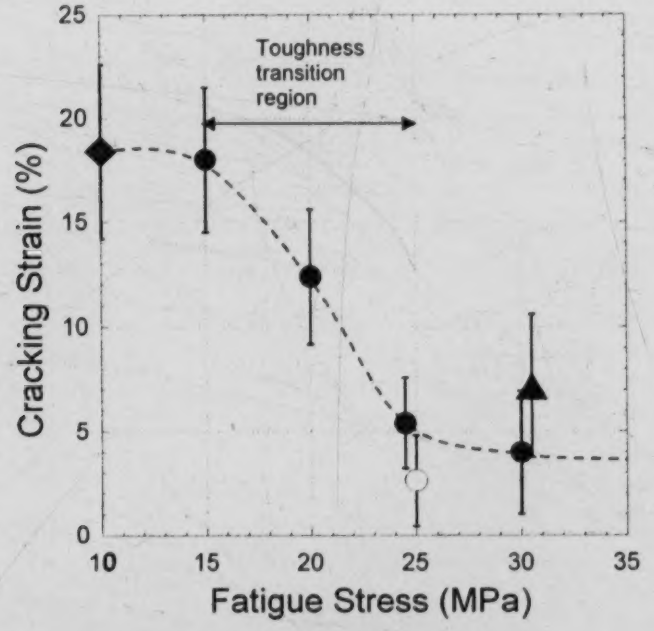

Fig. 4.2 Variation of cracking strain with uniaxial fatigue loading.
(◆: non-fatigued; ●: uniaxially fatigued with original thickness; ○: uniaxially fatigued with reduced thickness to 40%; ▲: non-equi-biaxially fatigued with original thickness, the biaxiality(σ_2/σ_1) is 0.25)

Introduction of Transverse Stress

The solid triangle (▲) in Fig. 4.2, at 30MPa, is the cracking strain for biaxially fatigued specimens that correspond to specimen 1 and 7 in Fig. 4.7. The biaxiality (σ_2/σ_1)

of this point is 0.2 (σ_1=30MPa, σ_2=6MPa), not 1.0. Though the transverse stress was not as high as that applied to the other biaxially fatigued specimens ($\sigma_2=\sigma_1$), it clearly shows the cracking strain higher than that for the uniaxially fatigued specimens by about 50%.

Biaxial Fatigue

The cracking strains after biaxial fatigue loadings (with the biaxiality of 1:1 except at 30MPa) are presented in Fig. 4.3 with the broken line (— - —) showing the trend. The trend from the uniaxially fatigued specimens is also included by dashed line (- - - -). The two curves show a similar trend, but the threshold fatigue stress for the biaxial specimens is above 20MPa that is higher than that for the uniaxial specimens by about 5MPa. Therefore, the major transition under the biaxial fatigue is shifted to the right by about 5MPa compared to that under the uniaxial fatigue.

Biaxial Fatigue with Reduced Thickness

It should be noted that the specimens for the biaxial fatigue stress of 25MPa in Fig. 4.3 had reduced thickness in the gauge section to 40% of the original thickness. As discussed in section 2.4, without the thickness reduction, the cruciform specimen could not survive at this level of the biaxial fatigue loading. As found in uniaxial fatigued specimens, the cracking strain with the original thickness is higher than that with the reduced thickness. Therefore, the cracking strain of the biaxially fatigued specimen with the original thickness should be higher than that shown by the open square (□) in Fig. 4.3. Consequently, the trend of the cracking strain variation for the biaxially fatigued specimens is estimated to be above the point of open square, as depicted in Fig. 4.3.

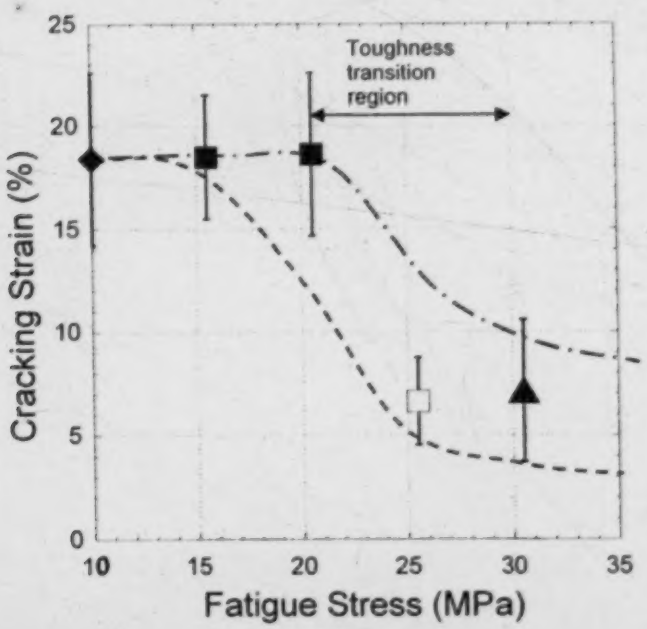

Fig. 4.3 Variation of cracking strain with uniaxial and biaxial fatigue loading.
(◆: non-fatigued; ■: biaxially fatigued with original thickness; □: biaxially fatigued with reduced thickness to 40%; ▲: non-equi-biaxially fatigued with original thickness, the biaxiality(σ_2/σ_1) is 0.25)

The Effect of Transverse Stress

As mentioned before, the solid triangle (▲) in Figs. 4.2 and 4.3, at 30MPa, is the cracking strain of specimens of the original thickness under the biaxiality of 0.25. Since it was impossible to generate the equi-biaxial fatigue stress of 30MPa with the current thickness reduction (60%) and more thickness reduction was impractical, the curve for the biaxially fatigued specimens in Fig. 4.3 in the stress range above 30MPa can only be speculated, based on the solid triangle point. The relative position of the solid circle and solid triangle points at 30MPa in Fig. 4.2 suggests that the increase of the transverse stress from 0MPa to 7.5MPa increases the cracking strain. It is reasonable to believe that a further increase of the transverse stress to 30MPa, if possible, would have resulted in an

even higher cracking strain. Thus, the trend of cracking strain for biaxial fatigue should lie above that for uniaxial fatigue, as shown in Fig. 4.3.

Discussion

The cracking strain lines in Fig. 4.2 and 4.3 suggest a general trend that the reduction of cracking strain after biaxial fatigue loadings is smaller than that after uniaxial fatigue loadings. The threshold stress for the uniaxial fatigue is lower than that for the biaxial fatigue. The biaxial fatigue loading also induced less cracking strain reduction than did the uniaxial loading across the transition region, which is 15 to 25MPa for the uniaxial fatigue, and 20 to 30MPa for the biaxial fatigue.

These results support the conclusion that the toughness drop after biaxial fatigue loading is smaller than that after uniaxial fatigue loading. In other words, the transverse stress increased the toughness of ABS subjected to the fatigue loading.

As discussed in section 1.4, two distinctively different conclusions were drawn about the effect of the transverse stress on the toughness. One suggested that the toughness increased with the application of the transverse loadings while the other suggested that the effect was adverse and there were no consistent conclusions. On the other hand, all of the previous studies used pre-cracked specimens. Those conclusions may not be applicable to crack initiation.

In the present study, un-notched specimens were used to measure cracking strain for the toughness evaluation. The results suggest that the existence of transverse loading increases the resistance to craze and crack initiation. The above conclusion can be applied to practical engineering designs when ABS is used for products under fatigue loadings. Our study suggests that fatigue resistance under uniaxial loading represents the lower

bound of the fatigue resistance under any combination of tensile fatigue loadings. It is yet to be verified whether other polymeric materials show the same fatigue-toughness characteristics as ABS.

4.4 Micro-structural analysis

4.4.1 Fracture deformation

As mentioned in chapter 1, it is generally known that fatigue fracture development consists of 4 phases [53]: (i) crack initiation, (ii) stage-I crack growth in the direction of maximum shear stress, (iii) stage-II crack growth in the direction of maximum tensile stresses, and (iv) ultimate fracture. These phases are represented diagrammatically in Fig. 4.4. However, the fracture development process does not fully represent the fracture process in our study, as the specimens were fractured under monotonic tension. Nevertheless, scanning electron microscopy (SEM) examination of the fracture surface did show fracture behavior similar to that shown in Fig. 4.4. Therefore, Fig. 4.4 is suitable for describing the fracture development process in our specimens. Fig. 4.5 is a SEM micrograph of a specimen that fractured in a very brittle manner during the tensile test, with a cracking strain of 3.5%, after 500 cycles of uniaxial fatigue loadings at 25MPa. This is a typical fracture surface of our specimens showing a significant drop in cracking strain after the fatigue loading above the threshold stress level.

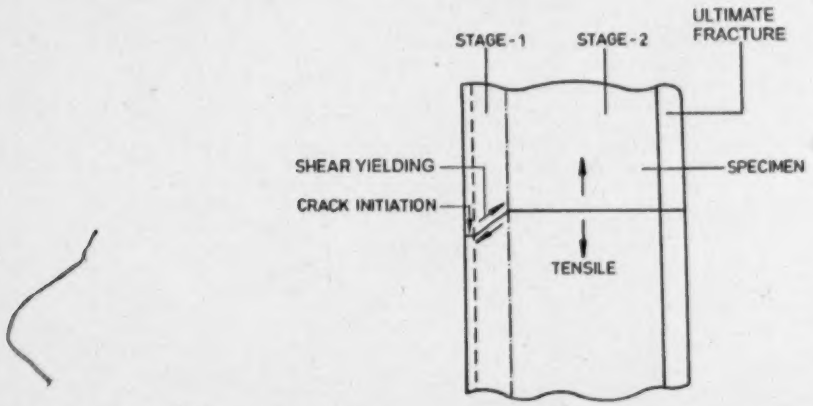

Fig. 4.4 Four phases of fracture development under fatigue loading [53]

4.4.2 Shear yielding and crazing

In Fig. 4.5, the diagonally shaded band from the top middle edge to the left bottom corner (D-D') is the border between the stage I and the stage II regions that were developed during the tensile test. The SEM micrographs from circle A are shown in Fig. 4.6. Fig. 4.6(a) was taken at low magnification, showing the overall tearing pattern that is typical for shear-deformation-dominated fracture in polymers. Bucknall [54] suggested that both crazing and shear yielding are toughening processes that can occur simultaneously in rubber-toughened plastics, but relative weighting of the two toughening mechanisms may vary among different materials. For example, in HIPS, crazing dominates and there is little evidence for shear yielding. In ABS, on the other hand, crazing and shear yielding can proceed simultaneously, so that ABS specimens exhibit both stress-whitening and necking in tension. For our specimens, the stress-whitening covered the whole fracture surface, which is the evidence of crazing. Fig. 4.6(b) is a SEM micrograph of high magnification from the same region (circle A in Fig. 4.5). In addition to the slanted wave-like fracture surface, the micrograph shows many

cavitated rubber particles.

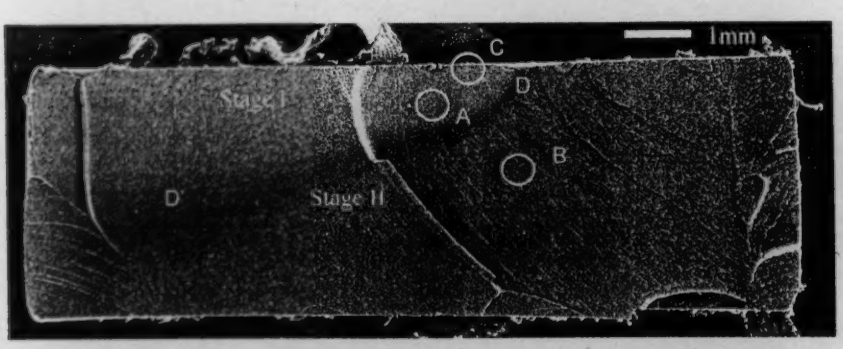

Fig. 4.5 SEM micrograph of tensile fractured surface, after 500 cycles of uniaxial fatigue loading at 25MPa (From specimen F-1)

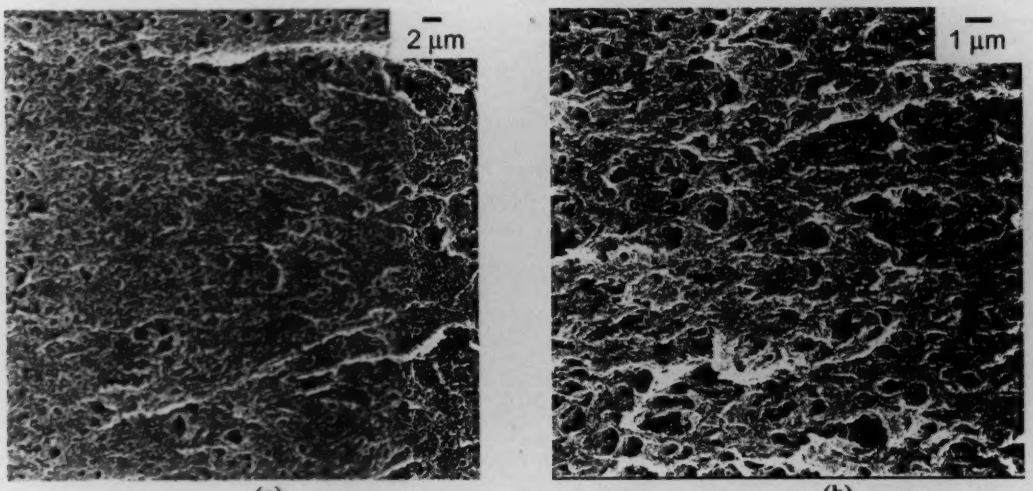

Fig. 4.6 SEM micrographs of fractured surface of an ABS specimen, from region A in Fig. 4.5. (a) Low magnification in stage I region, and (b) high magnification of the central region in (a).

According to the hypothesis of toughening processes proposed by Pearson and Yee [55, 56] and Bucknall [57], rubber cavitation took place first, followed by large-scale shear yielding of the matrix, i.e. without the cavitational process, the shear bands would not have formed. This process was also supported by the work of Sue et al. [58,59] in the

study of rubber-toughened polycarbonate and rubber-toughened epoxy. Fig. 4.7 is their proposed sequence of cavitation and shear yielding in rubber toughened polymers. The rubber particle cavitation reduced hydrostatic stress in front of the crack tip, which significantly altered the crack tip stress field to be in favor of shear yielding. The deformation process of local cavitation and then shear yielding is believed to continue to the shaded band (D-D') in Fig. 4.5, beyond which a different deformation process occurred.

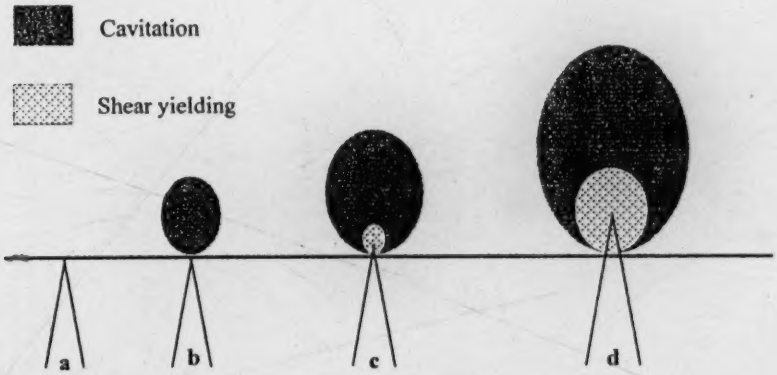

Fig. 4.7 Deformation sequence in front of the crack tip in rubber toughened polymers. (a) Initial crack tip; (b) formation of a cavitation zone in front of the crack tip when the specimen is loaded; (c) Formation of an initial shear yielded plastic zone in the cavitation zone due to the relief of hydrostatic tension by the rubber particle cavitation; (d) crack growth in the matured shear deformation zone [58]

The shear-yielding-dominated region of the pure tensile fractured specimens was closely examined using SEM to understand the shear yielding process. Fig. 4.8 presents a top view and a side view of a purely tensile fractured specimen. This specimen showed a very ductile fracture behavior with a large cracking strain, and the fracture surface contains a large shear-yielding-dominated region. The side view of the crack initiation shows a conical shape which agrees well with the prediction by Brady and Yeh [60] that

the angle between the shear band and the applied tensile stress should be approximately 60°. In our case, θ in Fig. 4.8(b), the angle of the shear band at the starting point with respect to the direction of the tensile force, is between 60° and 65°.

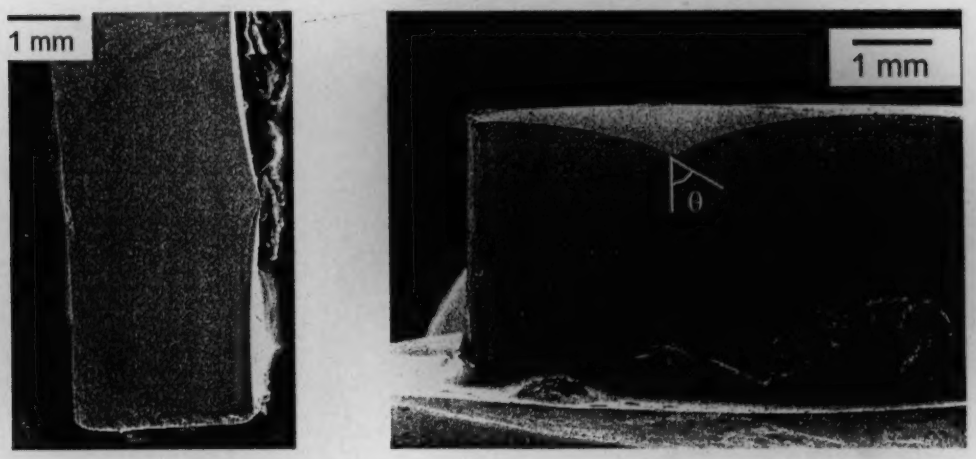

Fig. 4.8 SEM micrographs of the shear yielding dominated region of an ABS specimen fractured under pure tension

Fig. 4.9 shows a tilted view of the shear yielding dominated region. It shows the fractured surface in a thin planar region subjected to high shear strain. The slanted broken structures are explicitly shown.

As the fracture proceeded beyond the border of D-D', it is believed that the stress intensity factor (K_I) reached the critical value for fracture (K_{IC}) before the stress for shear yielding, which caused catastrophic failure instead of the steady ductile shear failure [61]. This corresponds to the Stage II crack growth and ultimate fracture region in Fig. 4.4. SEM micrograph from the region of circle B in Fig. 4.5 is shown in Fig. 4.10. The SEM micrograph showed very few cavitated rubber particles and fairly flat fracture surface, which is the evidence of crazing that dominated the fracture process.

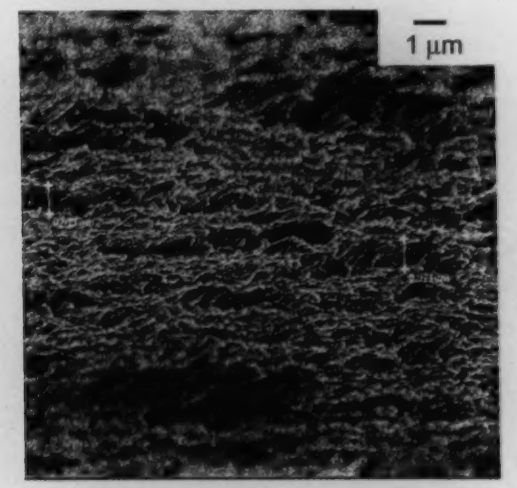

Fig. 4.9 SEM micrograph of a shear yielding dominated region of an ABS specimen fractured under pure tension.

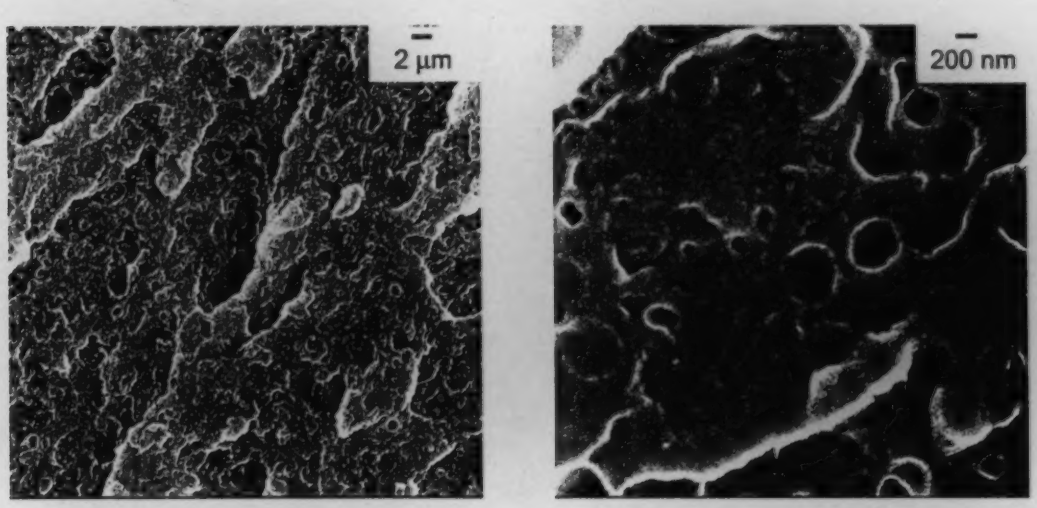

Fig. 4.10 SEM micrographs of fractured surface of an ABS specimen, from region B in Fig. 4.5. (a) crazing dominated stage II region, and (d) high magnification of the central region of (a).

The ABS used for this study has a bi-modal particle size distribution, one of around 1μm in diameter and the other around 0.1μm, which can be seen embedded in the matrix

in Fig. 4.10 (b). The bimodal particle size distribution is known to enhance the toughness of ABS [62,63].

Bucknall [45] suggested that shear yielding and crazing are two competing toughening mechanisms in ABS. When crazing dominates the deformation, the fracture is brittle and catastrophic. Toughness increases by increasing the involvement of shear yielding in the deformation process. Under certain stress conditions both mechanisms operate simultaneously, resulting in the interactions between the two deformation mechanisms. Several attempts have been made to establish a criterion to determine the fracture mode under various stress states and the associated failure envelope. Sternstein and Ongchin [64], based on the principle of the maximum strain in an isotropic body, suggested a critical strain condition for the crazing. That is, the maximum principal strain ε_1 reaches a critical value when crazing occurs. The criterion for the crazing can be expressed in terms of stress as

$$\sigma_{11} - \nu(\sigma_{22} + \sigma_{33}) = C(t,T) - D(t,T)/(\sigma_{11} + \sigma_{22} + \sigma_{33}) \qquad (4.1)$$

where ν is the Poisson's ratio, σ_{11}, σ_{22} and σ_{33} are principal stresses ($\sigma_{11} > \sigma_{22} > \sigma_{33}$), and $C(t,T)$ and $D(t,T)$ are time- and temperature- dependent constants.

On the other hand, the criterion for shear yielding is based on modified von-Mises yield criterion, suggested by Raghava [65], and can be written in terms of the principal stresses as

$$(\sigma_{11} - \sigma_{22})^2 + (\sigma_{22} - \sigma_{33})^2 + (\sigma_{33} - \sigma_{11})^2 + 2(\sigma_{ty} - \sigma_{cy})(\sigma_{11} + \sigma_{22} + \sigma_{33}) = 2\sigma_{ty}\sigma_{cy} \qquad (4.2)$$

where σ_{ty} and σ_{cy} are the tensile and compressive yield stresses at atmospheric pressure.

These equations can be plotted for PMMA in plane biaxial stress condition (σ_3=0) as Fig. 4.11. Having both the shear yielding and crazing envelopes on the same plot allows the prediction of the type of fracture that may occur under any general state of stress. For example, in the first quadrant of Fig. 4.11, under biaxial tension, the polymer fails by crazing as predicted by the critical tensile strain criterion, and subsequently fractures in a brittle manner at a stress well below that predicted for shear yielding. In the third quadrant, under biaxial compression, the polymer yields by shear yielding according to the von-Mises criterion; no crazing is possible. In the second and fourth quadrants, however, the two envelopes intersect, and there are conditions under which both crazing and shear yielding can occur simultaneously. Fig. 4.11 is the failure envelope for PMMA and it only gives us an idea how the failure mechanism changes during the fracture process. The shape of the failure envelope of ABS will be different from Fig. 4.11 with different asymptotes and intersects with x and y axis and Fig. 4.11 can not be used directly to explain the failure mechanism in ABS.

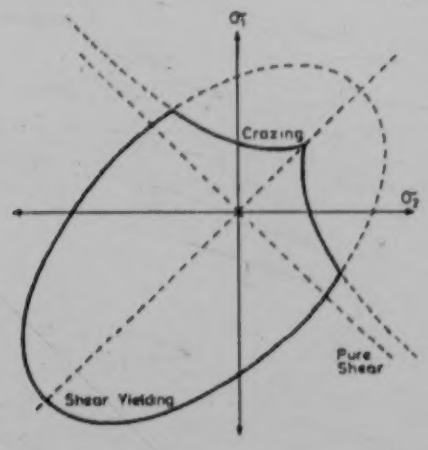

Fig. 4.11 Failure envelopes for PMMA under biaxial stress showing crazing and shear yielding (Raghava et al. [65])

However, Fig. 4.11 provides a clue as to why the dominating fracture mechanism switched from shear yielding to crazing. As the fracture proceeds, the local stress state was changing, and the coordinate in the failure envelope moved from the shear yielding dominated region to crazing dominated region.

4.4.3 Damage zone

Fig. 4.12 presents two SEM micrographs from circle C in Fig. 4.5, which contains the initiation zone of fracture. The fracture streamlines that stem from this region indicate that the fracture growth direction was initially perpendicular to the plate edge. A small shaded band can be found in the right part of Fig. 4.12(a), inside which a magnified view is shown in Fig. 4.12(b). The fracture behavior presented in Fig. 4.12(b) is different from that in Fig. 4.10(b) in that a significant number of small rubber particles of 0.1μm in diameter were debonded from the matrix in Fig. 4.12, but very few in Fig. 4.10. Both figures show the fracture of the large rubber particles of around 1μm in diameter, instead of cavitation, as shown in Fig. 4.6. We therefore believe that fracture mechanisms involved in Figs. 4.10 and 4.12 are similar, except that Fig. 4.12 contains debonding of small rubber particles, but Fig. 4.10 does not.

The region C in Fig. 4.5 must have formed during the fatigue loadings because this region could not be found in the pure tensile fractured specimens. The debonding of the small rubber particles could not be seen in Fig. 4.6 or Fig. 4.10; therefore, the debonding must have occurred during the fatigue loading. On the other hand, striations cannot be found in any samples examined in the study, suggesting that cracks did not grow during the fatigue loading.

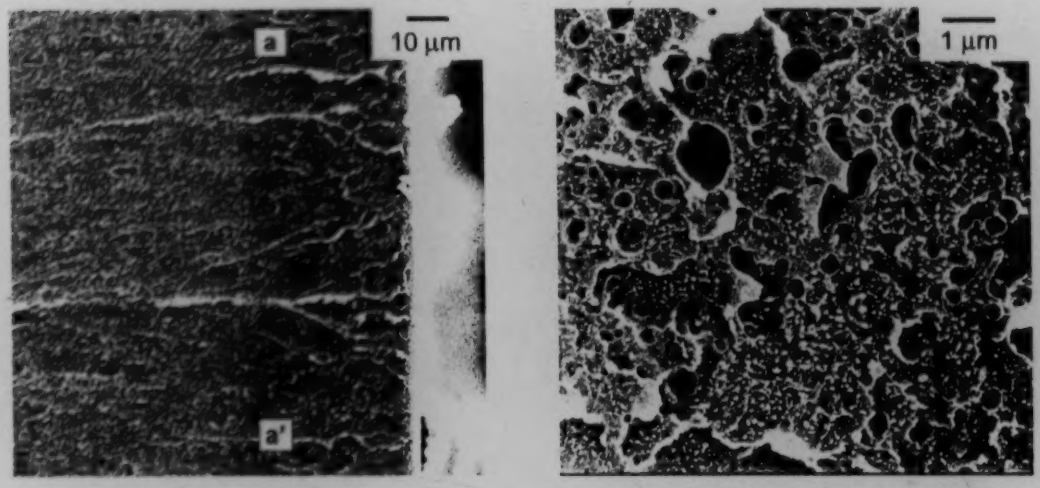

(a) (b)

Fig. 4.12 SEM micrograph of fractured surface of an ABS specimen, from region C in Fig 3.5. (a) Low magnification of the fracture starting area, and (b) high magnification of the region inside the band in (a).

The deformation mechanism in region C of Fig. 4.5 can be explained using the model presented in Fig. 4.13. Since the fatigue loading was around 50% of the yield strength, most of the matrix was experiencing repeated elastic deformation during the fatigue cycles. The elongation limit of the rubber is much larger than that of the matrix, and the rubber particles remained adhered to the matrix while the deformation of the matrix is in the elastic range. However, if there were defects and the concentrated stress around the defects were high enough to cause local yielding by crazing which is a highly localized deformation, cavitation and strains on the order of 100% [66,67,68,69] ccurred in the crazed area as shown in Fig. 4.14. Most crazes have a thickness (fibril length) around 0.1 μm [70] and thus the overall deformation created by crazes is very small while the local strains of the matrix around the crazes are very large. The large rubber particles of 1 μm in diameter could accommodate the matrix deformation and kept adhering to the

matrix, but the small rubber particles of 0.1 μm in diameter could not and were debonded from the matrix during fatigue loading. The fibrils are aligned packets of molecular chains and the aligned structure enables the fibrils to carry very high stresses relative to the undeformed state. Therefore, the yield strength does not drop even after crazes are formed. The shaded band (a-a') in Fig. 4.12(a) is believed to be the end of the area that was crazed during the fatigue loading. It should be noted that the region with fracture surface represented by Fig. 4.12(b) will be called "damage zone" in the remaining part of this thesis.

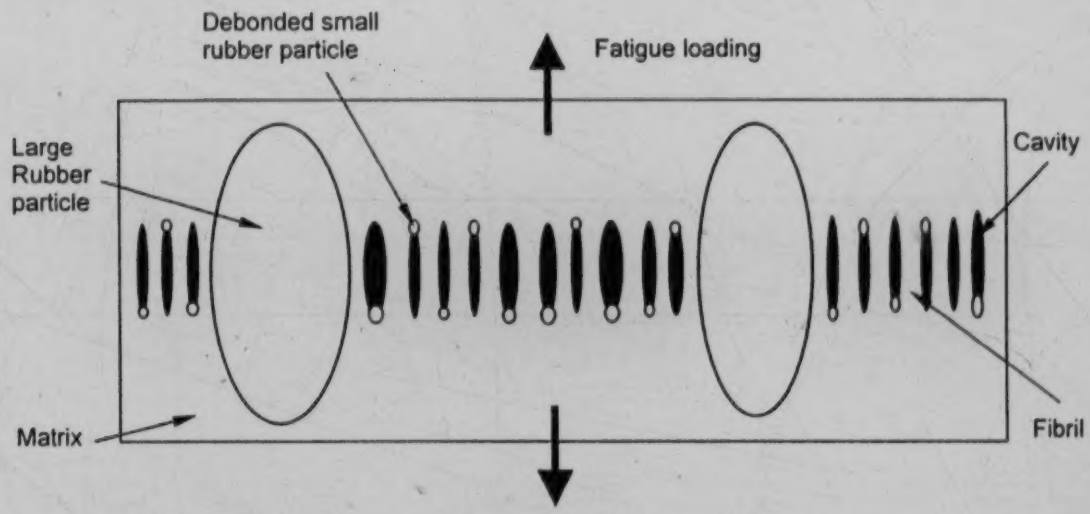

Fig. 4.13 Deformation model of a damage zone during the fatigue loading

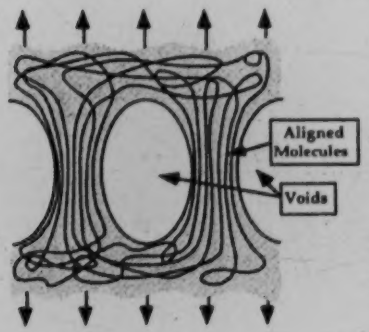

Fig. 4.14 Craze formation in glassy polymers. (Anderson [19])

The fracture surface of Fig. 4.12 was eventually formed during tensile test by breakdown of the fibrils in the craze and fracture of large rubber particles. Some of the large rubber particles were cavitated during the tensile test fracture. Since crazes were already formed during the fatigue loading, most of the large rubber particles were cleaved, similar to the craze-dominated region in Fig. 4.10(b). As a conclusion, the fatigue damage zone is not a crack but a locally crazed area in which the crack was formed during the tensile test.

Initiation of a damage zone might be from defects on the specimen surface. The defects could be the surface scratches or intrinsic defects such as rubber gel [71]. Since the stress around the defects was amplified during the fatigue loading, local plastic softening, through craze formation, occurred around the defects. If the fatigue loading level was too low, the amplified stress could not exceed the critical stress to generate the damage, and the toughness could not change. The threshold stress discussed in section 3.3 is the fatigue stress level required to generate the damage around the defects.

If the damage zone was a crack, it should propagate in a stable or unstable manner because the stress intensity factor (K_I) increases with the increase of crack length. Since the depth of damage zone was always limited to around 25μm, it should be a craze not a crack. Also, striation which is a proof of crack growth could not be found around the damage zones.

The initial defects on the surface for the stress amplification must have been related to the original surface finish of the specimens. Even if the surface finish for the specimens with original thickness is the same as that with the reduced thickness, the surface to the volume ratio was larger for the specimens with the reduced thickness.

Therefore, the specimen with the reduced thickness has a larger chance to develop the damage zone. This explains the decreasing trend of cracking strain with the decrease of thickness.

4.4.4 Toughness variation by fatigue loading

To know the effect of damage zone on the cracking strain, the fractured surface of another specimen (F-2) which shows very different cracking strains from the specimen (F-1) in Fig. 4.5 was investigated using SEM. Specimen F-2 underwent the same fatigue process (25MPa, 500 cycles) as specimen F-1 in Fig. 4.5, but fractured in a very different manner. Fig. 4.15 shows the over-all fracture surface of this specimen.

Specimen F-2 showed a very large cracking strain, 10.5%, while specimen F-1 showed the cracking strain of 3.5%. The difference is reflected by the fracture surface topography. Specimen F-1 contains several damage zones, but specimen F-2 contains only one damage zone. This strongly suggests that the remaining toughness after fatigue is closely related to the number and size of the damage zones generated during the fatigue, i.e. fatigue loading generates multiple damage zones that reduce the cracking strain for the following tensile fracture. The observation suggests that control of the surface defects, either surface scratches or containments, is an important factor to avoid fatigue-induced toughness drop of ABS.

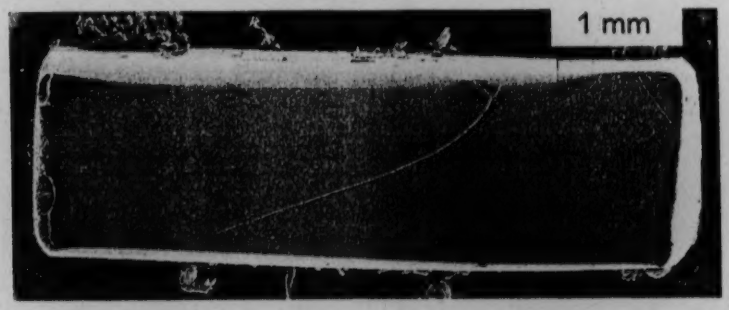

Fig. 4.15 SEM micrograph of a fractured surface from a purely tensile fractured ABS specimen (F-2) after 500 cycles of uniaxial fatigue loading at 25MPa

The smaller toughness drop from biaxial fatigue loading than that from uniaxial fatigue loading can be explained in the following way. Provided that these specimens have the same surface condition, both in types of defects and defect distribution, the only factor that can cause a different toughness drop is the stress field around the defects. Since there was no crack in the specimens after the fatigue loading, an explanation based on elasticity theory [72] can be used to explain the difference between the specimens after uniaxial fatigue loading and those after biaxial fatigue loading.

Assuming that the shape of the defects is circular, the stress field around the defect under the uniaxial loading state is expressed as follows:

$$\begin{aligned}
\sigma_r &= \frac{1}{2}\sigma_0\left[(1-\frac{a^2}{r^2})+(1+\frac{3a^4}{r^4}-\frac{4a^2}{r^2}\right]\cos 2\theta \\
\sigma_\theta &= \frac{1}{2}\sigma_0\left[(1+\frac{a^2}{r^2})-(1+\frac{3a^4}{r^4}\right]\cos 2\theta \qquad (4.3) \\
\tau_{r\theta} &= -\frac{1}{2}\sigma_0(1-\frac{3a^4}{r^4}+\frac{2a^2}{r^2})\sin 2\theta
\end{aligned}$$

where σ_0 is the remote uniaxial tensile stress. The stress distribution around a circular defect is depicted in Fig. 4.16. Since the initiation of the crack from the defect is

dependent on σ_θ and the maximum σ_θ under the uniaxial loading occurs along the y-axis which is 3 times of the remote stress, the crack initiation must start from the location where y-axis is. Along the edge of the circular hole in Fig. 4.16, σ_r and $\tau_{r\theta}$ are zero and σ_θ can be expressed as:

$$\sigma_\theta = \sigma_0(1-2\cos 2\theta) \qquad (4.4)$$

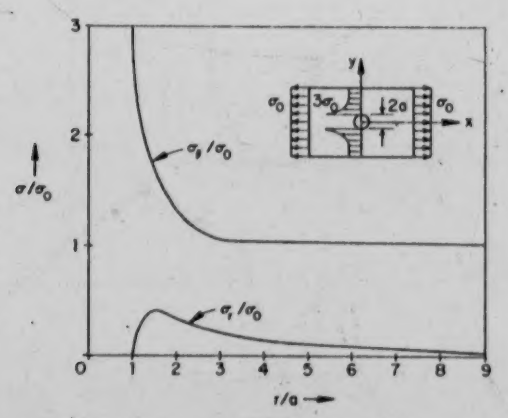

Fig. 4.16 Stress distribution, σ_r and σ_0, around the circular hole under the uniaxial loading [72]

Variation of the ratio of circumferential stress to the remote stress (σ_θ/σ_0) along the edge of the circular hole is depicted in Fig. 4.17 as a function of θ. The maximum σ_θ subjected to a remote uniaxial tensile stress of σ_0 is $3\sigma_0$; while the maximum σ_θ under the equi-biaxial tensile stress is $2\sigma_0$ by the superposition of the applied stresses in the two directions. Therefore, the maximum stress along the edge of the defect is reduced as the remote loading state changes from uniaxial to equi-biaxial. This should be the main reason for the larger cracking strain after biaxial fatigue loading. However, if an equi-biaxial stress state of tension-compression is introduced, Fig. 4.17(b), the ratio of maximum stress to remote stress (σ_θ/σ_0) under biaxial loading is larger than that under

pure uniaxial tension.

For practical engineering designs, an equi-biaxial stress state of tension-tension is the recommended loading condition and the tension-compression stress state should be avoided. This principle can be applied to other polymers that have shear yielding and crazing as two competitive mechanisms for deformation.

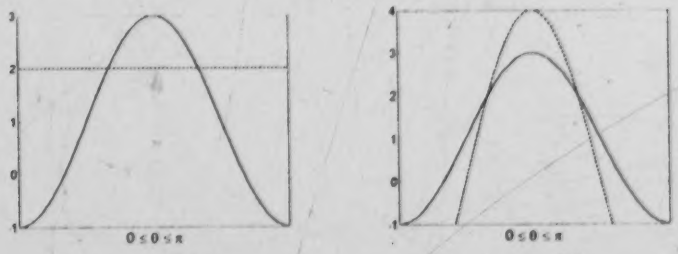

(a) (b)

Fig. 4.17 Distribution of σ_θ along the edge of the hole under uniaxial loading (——) and biaxial loading (-------).
Uniaxial tensile loading with (a) equi-biaxial tensile loading ($\sigma_1=\sigma_2=\sigma_\theta$), (b) biaxial tensile and compressive loading ($\sigma_1=\sigma_\theta$, $\sigma_2=-\sigma_\theta$))

4.4.5 Summary

The fracture surface of ABS specimen under fatigue can be divided into 3 regions: damage zone, shear-yielding-dominated region, and crazing-dominated-region. The damage zone doesn't contain a crack during the fatigue loading. It is a region where crazes were generated initially. The number and size of the damage zones determine the cracking strain in the following tensile test. Difference of the cracking strains among specimens under biaxial fatigue and uniaxial fatigue can be explained by stress distribution around the defect. The maximum stress around the defect under biaxial loading is less than that under uniaxial loading, which is the reason for less chance of

generating damage zones, i.e. less drop of cracking strain, for the biaxially fatigued specimens.

5. Conclusions

Toughness change of ABS after uniaxial and biaxial fatigue loadings was investigated using cracking strain values from the subsequent tensile tests. Micro-structural analysis was conducted to investigate the mechanisms of the toughness change. Based on the results, a deformation model under fatigue loading was presented which provided an explanation for the toughness change under uniaxial and biaxial fatigue loadings.

The conclusions reached from this study are as follows:

- The toughness drop can occur in ABS under fatigue loading even before any crack was developed.
- The toughness drop after the biaxial fatigue loading is smaller than that after the uniaxial fatigue loadings. The results suggest that the existence of transverse stress increases the toughness for crack initiation in ABS.
- SEM micrographs show that the tensile fractured surface consists of deformation in 4 phases: damage zone, shear-yielding-dominated region, crazing-dominated-region and ultimate fracture. Shear yielding and crazing are competing fracture mechanisms in ABS and the dominating mechanism was found to be shear yielding in the early stage of crack growth, which was later transformed to crazing.

- In the shear-yielding-dominated region, the shear deformation followed extensive particle cavitation. However, in the crazing dominated region, much less cavitation occurred and the fracture was in a brittle manner.
- Micro-structural analysis revealed that the toughness drop came from the small damage zones. Since the damage zones could not be found on the fracture surface of pure tensile fractured specimen or the fatigued fractured specimen subjected to loading less than the threshold stress, the damage zones must have been initiated during the fatigue loading above the threshold stress.
- A deformation model for the damage zone was presented. The damage zone was initiated mainly from the surface defects, consisting of matrix crazes with debonding of small rubber particles. Large rubber particles of 1μm in diameter were cleaved in the following tensile tests, along with matrix cracks evolved from the crazes.
- The equi-biaxial tensile fatigue stress induces less stress concentration than the uniaxial counterpart. This is believed to be the reason for a smaller number of damage zones and a smaller toughness decrease of ABS under the biaxial fatigue loading.

6. Recommendations for the future studies

1) Fatigue loading in the current study is limited to 500 cycles, because of the limited availability of the testing equipment. It will be interesting to extend the study to include fatigue loading of low stress but an increased number of fatigue cycles.
2) ABS has the fracture mechanisms of both shear yielding and crazing that can occur simultaneously. In some materials, on the other hand, one of the mechanisms may dominate the fracture process. Further study can verify whether the observed trend of toughness drop exists in other materials that have different deformation mechanisms dominating the fracture process.
3) The nature of the damage zones generated during the fatigue loading could not be properly characterized in this study. Further investigation to characterize the structure in the damage zone and the associated loading conditions can be of great interest and complementary to the current study.

7. Bibliography

[1] S. P. Timosenko and J. M. Gere, "Theory of elastic stability", pp. 357, McGrawHill, New York (1961)

[2] E. W. Smith and K.J. Pascoe, "The behavior of fatigue cracks subject to applied biaxial stress: A review of experimental evidence", Fatigue of Engineering Materials and Structures, Vol. 6, No. 3, pp. 201 (1983)

[3] J. G. Williams, "Fracture Mechanics of Polymers", Ellis Horwood, Chichester (1984)

[4] R. W. Hertzberg and A. Manson, "Fatigue of Engineering Plastics", Academic Press, New York (1980)

[5] P. C. Paris and G. C. Sih, "Stress analysis of cracks", Fracture toughness testing and its applications, ASTM Special Technical Publication No. 381, pp. 30 (1964)

[6] P. S. Leevers, J. C. Radon and L. E. Culver, "Crack growth in plastic panels under biaxial stress", Polymer, Vol. 17, pp. 627 (1976)

[7] P. S. Leevr, L. E. Culver and J. C. Radon, " Fatigue crack growth in PMMA and rigid PVC under biaxial stress", Engineering Fracture Mechanics, Vol. 11, pp. 487 (1979)

[8] M. T. Takemori, "Biaxial impact fatigue of polycarbonate", Journal of Materials Science, Vol. 17, pp. 164 (1982)

[9] A. G. Atkins, G. Jeronimidis and S. Arndt, "Biaxial monotonic and fatigue fracture of some commercial ABS and PVC sheets", Journal of Materials Science, Vol. 33, pp. 4349 (1998)

[10] J. D. Embury and G. H. Leroy, Proc. ICF-4, 1, 15 (1977)

[11] H. A. Richard, in "Biaxial and Multiaxial Fatigue", EGF Publication 3. MEP, London, 217

[12] E. W. Smith and K. J. Pascoe, "The behavior of fatigue cracks subject to applied biaxial stress: A review of experimental evidence", Fatigue of Engineering Materials and Structures, Vol. 6, pp. 201 (1983)

[13] M. W. Parsons and K. J. Pascoe, "Observations of surface deformation, crack initiation and crack growth in low cycle fatigue under biaxial stress", Materials Science and Engineering, Vol. 22, pp. 31 (1976)

[14] K. J. Miller and A. P. Kfouri, "An elastic-plastic finite element analysis of crack tip fields under biaxial loading conditions", International Journal of Fracture, Vol. 10, pp. 393 (1974)

[15] P. J. E. Forsyth, "A two stage-process of fatigue crack growth", Proceedings of the Propagation Symposium, pp. 76, Cranfield (1961)

[16] B. Cotterell and J. K. Reddel, "The essential work of plane stress ductile fracture", International Journal of Fracture, Vol. 13, No. 3, pp. 267 (1977)

[17] A. A. Griffith, 'The phenomena of rupture and flow in solids", Philosophical Transactions, Series A. Vol. 221, pp. 163 (1920)

[18] C. E. Inglis, "Stresses in a plate due to the presence of cracks and sharp corners", Transactions of the Institute of Naval Architects, Vol. 55, pp. 219 (1913)

[19] T. L. Anderson, "Fracture Mechanics", CRC Press, USA (1995)

[20] G. R. Irwin, "Onset of fast crack propagation in high strength stel and aluminum alloys", Sagamore Research Conference Proceedings, Vol. 2, pp. 289 (1956)

[21] H. M. Westergaard, "Bearing pressures and cracks", Journal of Applied Mechanics, Vol. 6, pp. 49 (1939)

[22] M. L. Williams, "On the stress distribution at the base of a stationery crack", Journal of Applied Mechanics, Vol. 24, pp. 109 (1957)

[23] J. F. Knott, "Fundamentals of Fracture Mechanics", London Butterworths, UK (1973)

[24] A. P. Kfouri, "A crack in a linear-elastic material under mode II loading, revisited", Fatigue Fracture of Engineering Materials and structures, Vol. 22, pp. 445

[25] J. Lai and E. Van der Giessen, "A numerical study of crack-tip plasticity in glassy polymers", Mechanics of Materials", Vol. 25, pp. 183 (1997)

[26] C. F. Shih, "Relationship between the J-integral and the crack opening displacement for stationary and extending cracks", Journal of mechanics and physics and solids, Vol. 29, pp. 305 (1981)

[27] A. A. Wells, "Unstable crack propagation in metals: Cleavage and fast fracture", Proceedings of the Crack Propagation Symposium, Vol. 1, pp. 84, Cranfield, UK (1961)

[28] J. R. Rice, "A path independent integral and the approximate analysis of strain concentration by notches and cracks", Journal of Applied Mechanics, Vol. 35, pp. 379 (1968)

[29] J. A. Begley and J. D. Landes, "The J-integral as a fracture criterion", ASTM STP 514, American Society for Testing and Materials, Philadelphia, pp.24 (1972)

[30] J. R. Rice, P. C. Paris and J. G. Merkle, "Some further results of J-integral analysis and estimates", ASTM STP 536, American Society for Testing and Materials, Philadelphia, pp.231 (1973)

[31] K. B. Broberg, "Critical review of some theories in fracture mechanics", International Journal of Fracture Mechanics, Vol. 4, pp. 11 (1968)

[32] K. B. Broberg, "Crack-growth criteria and non-linear fracture mechanics", Journal of the Mechanics and Physics of Solids, Vol. 19, pp. 407 (1971)

[33] K. B. Broberg, "On stable crack growth", Journal of the Mechanics and Physics of Solids, Vol. 23, pp. 215 (1975)

[34] E. Orowan, "Fundamentals of Brittle Behavior in Metals", Fatigue and Fracture of Metals, Wiley, New York (1950)

[35] B. Cotterell and J. K. Reddel, "The essential work of plane stress ductile fracture", International Journal of Fracture, Vol. 13, No. 3, pp. 267 (1977)

[36] R. J. Young and P. A. Lovell, "Introduction to Polymers", 2nd ed., Champman & Hall, U.K. (1991)

[37] G. F. Giaconi, L. Castellani, C. Maestrini and T. Ricco, "Development of toughness in ABS resins", Polymer, Vol. 39, pp. 6315 (1998)

[38] F. Ramsteiner, W. Heckmann, G. E. Mckee and M. Breulumann, "Influence of void formation on impact toughness in rubber modified styrenic-polymers", Polymer, Vol. 43, pp. 5995 (2002)

[39] Richard Lee, "Toughening mechanisms and deformation behavior of high-thermal-resistant poly(Acrylonitrile-Butadiene-Styrene)(ABS)", Master thesis, The Austrian National University (1999)

[40] E. Crawford and A. J. Lesser, "Mechanics of rubber particle cavitation in toughened polyvinylchloride", Polymer, Vol. 41, pp. 5865 (2000)

[41] E. Mönch and D.Galster, "A method for producing a defined uniform biaxial tensile stress field", British Journal of Applied Physics, Vol. 14, pp. 810 (1963)

[42] L. Cridland and W.G. Wood , "A hydrostatic tension test of a brittle material", The International Journal of Fracture Mechanics, Vol. 4, No. 3, pp. 277, (September 1968)

[43] S. R. Joshi and J.Shewchuk, "Fatigue-crack propagation in a biaxial stress field", Experimental Mechanics, Vol. 10, pp. 529 (1970)

[44] D. R. Hayhurst , "A biaxial-tension creep-rupture testing machine", Journals of Strain Analysis, Vol. 8, No. 2, pp. 119 (1973)

[45] D. A. Kelly, "Problems in creep testing under biaxial stress systems", Journals of Strain Analysis, Vol. 11, No. 1, pp. 1 (1976)

[46] C. D. Hopper and K.J. Miller, "Fatigue crack propagation in biaxial stress fields", Journal of Strain Analysis, Vol. 12, No. 1, pp. 23 (1977)

[47] H. Kitagawa and R. Yuuki, "A fracture mechanics approach to high-cycle fatigue crack growth under in-plane biaxial loads", Fatigue of Engineering Materials and Structure, Vol. 4, No. 4, pp. 355 (1981)

[48] T. Hoshide and K. Tanaka, "Stress-ratio effect of fatigue crack propagation in a biaxial stress field", Fatigue of Engineering and Structures, Vol. 2, pp. 195 (1979)

[49] P. S. Leevers, L.E. Culver and J.C. Radon, "Crack growth in plastic panels under biaxial stress", Polymer, Vol. 17, pp. 627 (1976)

[50] P. C. Paris, M. P. Gomez, and W.P. Anderson, "A rational analytic theory of fatigue", The Trend in Engineering, Vol. 13, pp. 9 (1961)

[51] P. C. Paris and F. Erdogan, "A critical analysis of crack propagation laws", Journal of Basic Engineering, Vol. 85, pp. 527 (1960)

[52] T.-J. Chen, C. P. Bosnyak, C.-I. Kao and A. Chudnovsky, "A Fatigue crack initiation map for polycarbonate", Journal of Applied Science, Vol. 49, pp. 1909 (1993)

[53] S. A. Meguid, "Engineering Fracture Mechanics", pp. 76, Elsevier Applied Science (1989)

[54] C. B. Bucknall, "Toughened Plastics", Applied Science, London, pp. 193 (1977)

[55] R. A. Pearson and A.F. Yee, "Toughening mechanisms in elastomer-modified epoxies", Journal of Materials Science, Vol. 21, pp. 2475 (1986)

[56] R. A. Pearson and A. F. Yee, "Influence of particle size and particle size distribution on toughening mechanisms in rubber-modified epoxies", Journal of materials science, Vol. 26, pp. 3828 (1991)

[57] C. B. Bucknall and et al., "Rubber toughening of plastics", Journal of Materials Science, Vol. 16, pp. 2255 (1989)

[58] D. S. Parker, H-J. Sue, J. Huang and A. F. Yee, "Toughening mechanisms in core-shell rubber modified polycarbonate", Polymer, Vol. 31, pp. 2267 (1990)

[59] Hung-Sue Sue, "Study of rubber-modified brittle epoxy systems. Part2: toughening mechanisms under mode-I fracture", Polymer Engineering and Science, Vol. 31, No. 4, pp. 275 (1991)

[60] T. E. Brady and G. S. Y. Yeh, "Yielding behavior of glassy amorphous polymers", Journal of Applied Physics, Vol. 42, pp. 4622 (1971)

[61] Keqin Xiao, "Fracture Behavior Rubber-Modified Epoxies and their Carbon Fibre-Reinforced Composites", PhD. Thesis, pp. 19 (2000)

[62] E. H. Rowe and C. K. Riew, "Failure mechanisms in rubber toughened thermoset resins", Society of Plastic Engineers, Annual Technical Conference Paper, Vol. 20, pp. 663 (1974)

[63] E. H. Rowe and C. K. Riew, "What failure mechanism tell about toughened epoxy resins", Plastics Engineering, Vol. 31, pp. 45 (1975)

[64] S. S. Sternstein and L. Ongchin, ACS Polymer, Vol. 10(2), pp. 1117 (1969)

[65] R. Raghava, R.M. Caddell and G. S. Y. Yeh, "The macroscopic yield behavior of polymers", Journal of Materials Science, Vol. 8, pp. 225 (1973)

[66] A. M. Donald and E. J. Kramer, "The mechanisms for craze-tip advance in glassy polymers", Philosophical Magazine A, Vol. 43, No. 4, pp. 857

[67] A. M. Donald and E. J. Kramer, "Effect of molecular entanglements on craze microstructure in glassy polymers", Journal of Polymer Science: Polymer Physics, Vol. 20, pp. 899 (1982)

[68] A. M. Donald and E. J. Kramer, "Internal structure of rubber particles and craze break-down in high-impact polystyrene (HIPS)", Journal of materials science, Vol. 17, pp. 2351 (1982)

[69] H. H. Mechler and C. B. Bucknall, "New toughening mechanisms in rubber modified polymers", Plastics, Rubber and Composites, Vol. 30, No. 3, pp. 110

[70] R. P. Kambour and R. W. Kopp, Journal of Polymer Science, Part A-2: Polymer physics, Vol. 7, pp. 183 (1969)

[71] P. -Y. B. Jar, A. J. Berry, K. Konishi and T. Shinmura, "Fracture initiation in emulsion-polymerized poly(arcylonitrile-butadiene-stryene)(ABS)", Journal of Materials Science Letters, Vol. 20, pp. 655 (2001)

[72] A. C. Ugral and S. K. Fenster, "Advanced Strength and Applied Elasticity", Elsevier (1975)